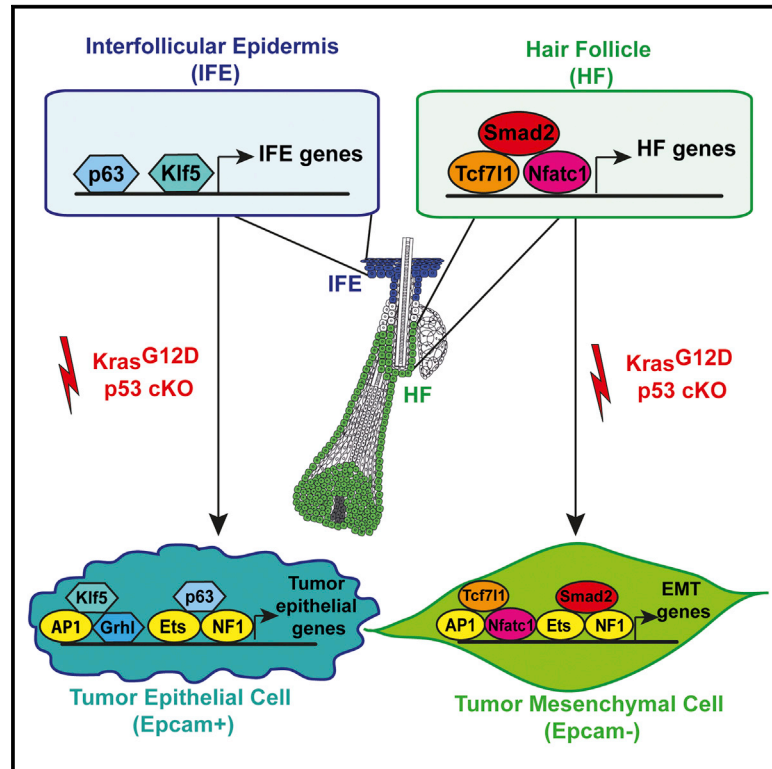# Cell Stem Cell

Cell-Type-Specific Chromatin States Differentially Prime Squamous Cell Carcinoma Tumor-Initiating Cells for Epithelial to Mesenchymal Transition

Graphical Abstract

Authors
Mathilde Latil, Dany Nassar, Benjamin Beck, ..., Wim Declercq, Rui Yi, Cédric Blanpain

Correspondence
cedric.blanpain@ulb.ac.be

In Brief

Latil and colleagues show that tumor phenotypes and propensity for EMT are dictated by cell-type-specific chomatin and transcriptional states of the cancer cell of origin. These findings provide insight into mechanisms through which chromatin landscapes and gene regulatory networks prime tumor-initiating cells to undergo EMT.

Highlights

- The cancer cell of origin controls EMT

- Transcriptional priming of EMT occurs in the cancer cell of origin

- Epigenetic priming of EMT occurs in the cancer cell of origin

- p63 restricts EMT in the cancer cell of origin

CrossMark

CellPress

Article

Cell-Type-Specific Chromatin States Differentially Prime Squamous Cell Carcinoma Tumor-Initiating Cells for Epithelial to Mesenchymal Transition

Mathilde Latil,[1,6] Dany Nassar,[1,6] Benjamin Beck,[1] Soufiane Boumahdi,[1] Li Wang,[2] Audrey Brisebarre,[1] Christine Dubois,[1] Erwin Nkusi,[1] Sandrine Lenglez,[1] Agnieszka Checinska,[1] Alizée Vercauteren Drubbel,[1] Michael Devos,[3,4] Wim Declercq,[3,4] Rui Yi,[2] and Cédric Blanpain[1,5,7,*]

[1]Université libre de Buxelles (ULB), Institut de recherche interdisciplinaire en biologie humaine et moléculaire (IRIBHM), 808 route de Lennik, 1070 Brussels, Belgium
[2]Department of Molecular, Cellular, and Developmental Biology, University of Colorado Boulder, Boulder, CO 80309, USA
[3]VIB Inflammation Research Center, Technologiepark 927, 9052 Ghent, Belgium
[4]Department of Biomedical Molecular Biology, Ghent University, Technologiepark 927, 9052 Ghent, Belgium
[5]WELBIO, Université Libre de Bruxelles (ULB), 1070 Bruxelles, Belgium
[6]Co-first author
[7]Lead Contact
*Correspondence: cedric.blanpain@ulb.ac.be
http://dx.doi.org/10.1016/j.stem.2016.10.018

SUMMARY

Epithelial to mesenchymal transition (EMT) in cancer cells has been associated with metastasis, stemness, and resistance to therapy. Some tumors undergo EMT while others do not, which may reflect intrinsic properties of their cell of origin. However, this possibility is largely unexplored. By targeting the same oncogenic mutations to discrete skin compartments, we show that cell-type-specific chromatin and transcriptional states differentially prime tumors to EMT. Squamous cell carcinomas (SCCs) derived from interfollicular epidermis (IFE) are generally well differentiated, while hair follicle (HF) stem cell-derived SCCs frequently exhibit EMT, efficiently form secondary tumors, and possess increased metastatic potential. Transcriptional and epigenomic profiling revealed that IFE and HF tumor-initiating cells possess distinct chromatin landscapes and gene regulatory networks associated with tumorigenesis and EMT that correlate with accessibility of key epithelial and EMT transcription factor binding sites. These findings highlight the importance of chromatin states and transcriptional priming in dictating tumor phenotypes and EMT.

INTRODUCTION

EMT is associated with cancer metastasis, tumor stemness, and resistance to therapy (Mani et al., 2008; Nieto et al., 2016; Yang et al., 2004). While the cancer cell of origin has been suggested to control tumor heterogeneity, no study has demonstrated so far that the cancer cell of origin controls EMT (Nieto et al., 2016). Depending on the cancer cell of origin (multipotent and unipotent stem cells, progenitors, and differentiated cells) initially targeted by oncogenic hits, different tumor phenotypes may arise, differing by their differentiation, aggressiveness, and EMT features.

The skin epidermis is an ideal model to assess whether the cancer cell of origin controls EMT, as it is composed of spatially distinct cell lineages including the interfollicular epidermis (IFE), the hair follicle (HF), and its associated sebaceous glands, as well as the infundibulum that connects the HF to the IFE (Blanpain and Fuchs, 2014) (Figure 1A). During homeostasis, each of these distinct epidermal lineages is self-sustained by its own pool of resident stem cells (SCs) that can be genetically targeted by specific CreER mice (Blanpain and Fuchs, 2014), allowing the conditional expression of oncogenes or deletion of tumor suppressor genes in different epidermal lineages and the assessment of their capacity to induce tumor formation (Blanpain, 2013). In studying the cellular origin of skin SCCs, the second most frequent skin cancer in humans, it has been previously demonstrated that oncogenic KRas expression combined with p53 deletion in IFE cells as well as in HF lineages leads to the development of different types of invasive SCCs, sometimes associated with EMT features, demonstrating that different epidermal lineages including the IFE and the HF were competent to induce skin SCCs (Lapouge et al., 2011; White et al., 2011). However, it remains unclear to what extent the cellular origin of skin SCCs influences EMT in these tumors.

Here, we used genetically engineered mouse models coupled with lineage tracing to assess whether the same oncogenic hits in different cell lineages of the skin epidermis influence EMT. Interestingly, HF-derived tumors are much more prone to undergo EMT as compared to IFE-derived tumors. Chromatin and transcriptional profiling of these two different epidermal populations during tumorigenesis revealed that the epigenetic and transcriptional landscapes of the cancer cell of origin primed oncogene-targeted cells to develop into either well-differentiated SCCs or more invasive tumors characterized by EMT,
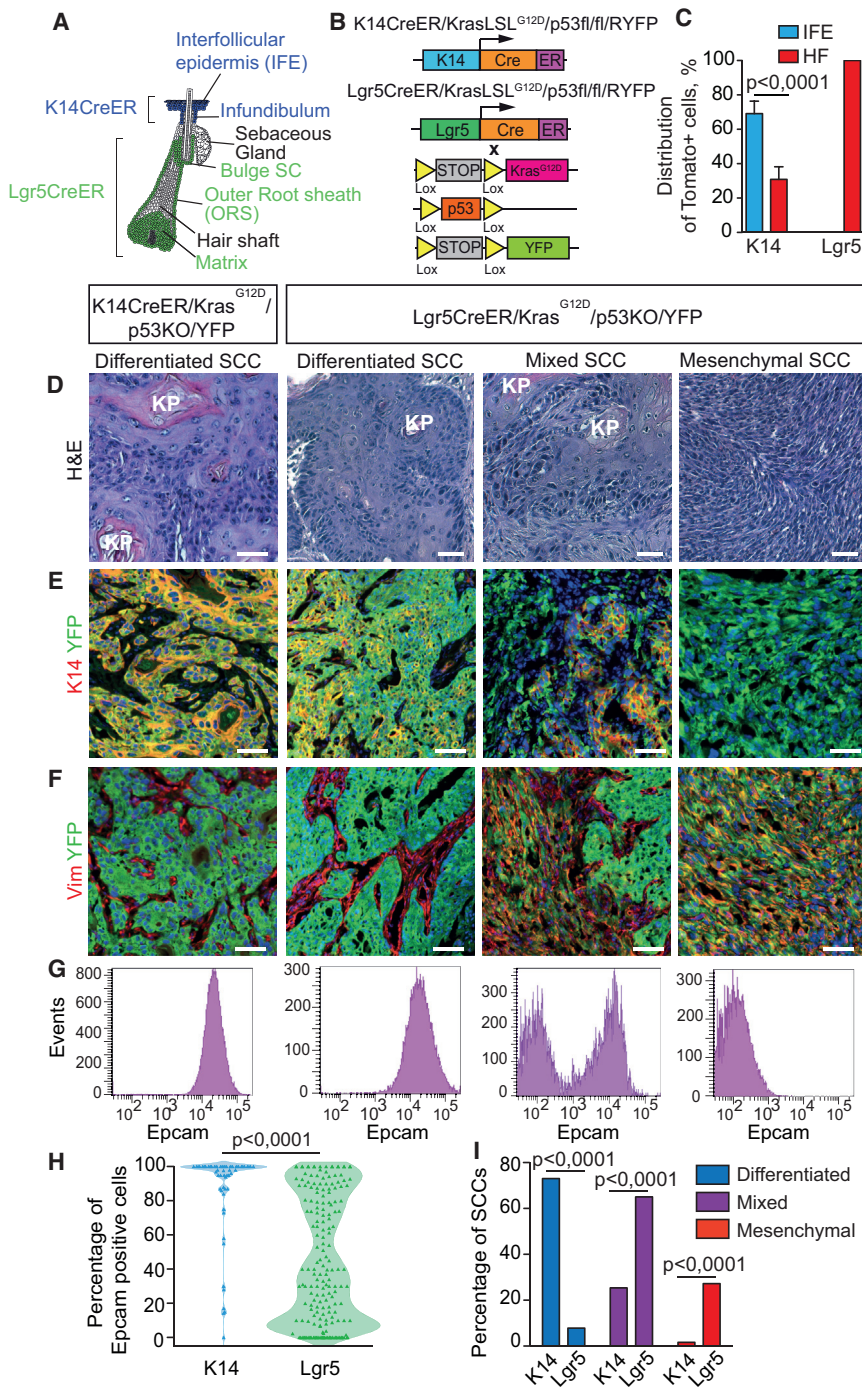
Figure 1. The Cellular Origin Controls EMT in Skin SCC

(A) Scheme of the skin epidermis and its different lineages.

(B) Mouse models of skin SCCs allowing the expression of YFP and Kras^{G12D} as well as p53 deletion preferentially in the interfollicular epidermis (IFE) using K14CreER or in the HF SCs and their progeny using Lgr5CreER.

(C) Graph showing the distribution of Tomato-positive cells counted on tissue sections in IFE and HF in K14CreER/Rosa-tdTomato and Lgr5CreER/Rosa-tdTomato 3 days after TAM administration (n = 1,729 cells from four K14CreER and n = 980 cells from four Lgr5CreER mice). Histogram represents mean ± SEM.

(D–F) Hematoxylin and Eosin (H&E) (D) and co-immunostaining of YFP and Keratin 14 (K14) (E) or Vimentin (F) in the different SCC subtypes. Scale bars, 50 μm.

(G and H) FACS profile (G) and quantification of the percentage of Epcam positive cells (H) in the different SCCs subtypes.

(I) Graph showing the proportion of differentiated, mixed, and mesenchymal tumors in K14CreER (n = 63) and Lgr5CreER (n = 192) mice.

K14CreER mice (K14CreER/KRas^{G12D}/p53$^{fl/fl}$/Rosa-YFP), in which low-dose tamoxifen (TAM) administration preferentially targets the IFE and the infundibulum (Lapouge et al., 2011) or in HF SCs and their progeny using Lgr5CreER mice (Lgr5CreER/KRas^{G12D}/p53$^{fl/fl}$/Rosa-YFP) (Lapouge et al., 2012) (Figures 1A–1C and S1A–S1D). These two CreER targeted exclusively epidermal cells and not mesenchymal cells in the skin (Figures S1A–S1D). The Rosa-YFP reporter gene was included in these different mouse models to track on tissue sections and isolate by fluorescence-activated cell sorting (FACS) YFP$^+$ tumor cells, including those that may have lost the expression of markers of their cell of origin (Figure 1B). As previously described (Lapouge et al., 2011), the kinetic of tumor appearance (around 6–9 weeks) and initial tumor growth rate were similar in K14- and Lgr5-derived tumors. However, Lgr5CreER mice developed more tumors than K14CreER mice (Figures S2E–S2G). Histological analyses revealed that K14-derived tumors were mostly well-differentiated SCCs, containing numerous keratin pearls. In contrast, tumors arising from Lgr5CreER/KRasG12D/p53$^{fl/fl}$/Rosa-YFP mice were composed of distinct phenotypes (Figure 1D). The most frequent tumor phenotype consisted of mixed tumor containing YFP$^+$ tumor epithelial cells (TECs) and YFP$^+$ tumor mesenchymal-like cells (TMCs), resembling human carcinosarcoma for which the epithelial or the mesenchymal origin remains an open

underscoring the importance of the cancer cell of origin in controlling EMT.

RESULTS

The Cancer Cell of Origin Controls EMT in Skin SCC

To determine whether the cancer cell of origin controls EMT in skin tumors, we assessed the tumor phenotypes following KRas^{G12D} expression and p53 deletion either in the IFE using

question (Paniz-Mondolfi et al., 2015). The other tumors included well-differentiated SCCs resembling the SCCs arising in K14CreER mice and tumors that were completely mesenchymal and called spindle cell carcinoma (Figure 1D). Well-differentiated SCCs, regardless of whether they originate from K14CreER or Lgr5CreER cells, expressed classical epidermal markers including K14, Epcam, and E-cadherin, and no YFP+ TECs expressed the mesenchymal marker Vimentin, which was only expressed by YFP-negative cancer-associated fibroblasts that composed the tumor stroma (Figures 1E, 1F, and S1H). In Lgr5-derived mixed SCCs, the well-differentiated part of the tumor expressed epithelial markers K14, Epcam and E-cadherin (Figures 1E and S1H). However, many cells located in the underlying mesenchymal part of the tumor were YFP+ TMCs that had completely lost the expression of all classical epithelial markers and expressed Vimentin (Figures 1E, 1F, and S1H). Likewise, in Lgr5-derived mesenchymal tumors, YFP+ TMCs and mesenchymal stromal cells were morphologically indistinguishable and were all K14, Epcam, and E-cadherin negative (Figures 1E, 1F, and S1H). FACS analysis of Epcam expression showed that the vast majority of YFP+ TECs in well-differentiated SCCs, whether K14 or Lgr5-derived, expressed high levels of Epcam (Figure 1G). Epcam expression was always bimodal in mixed tumors with two distinct YFP+ Epcam+ TEC and YFP+ Epcam− TMC populations, while in mesenchymal tumors all YFP+ TMCs were Epcam− (Figure 1G). FACS quantification of the proportion of YFP+ Epcam+ TECs and YFP+ Epcam− TMCs in a large number of tumors showed that the majority of K14-derived tumors (75%, n = 63) were well-differentiated SCCs composed of Epcam+ cells (Figures 1H and 1I). In contrast, the vast majority of Lgr5-derived tumors (92%) were composed of cells that had partially (mixed tumors) (65%, n = 224) or completely (mesenchymal tumors) (27%, n = 94) undergone EMT (Figures 1H and 1I). A similar degree of EMT was also observed upon Kras^{G12D} and p53 recombination using two other HF-specific inducible CREs (K15CrePR and K19CreER) (Lapouge et al., 2011) (Figure S1I), further demonstrating that the mesenchymal part of the tumor arises from the HF lineages. RT-PCR and PCR analysis of the Kras^{G12D} and p53 floxed alleles showed that KRas was expressed at similar level in TECs and TMCs and that both alleles were equally recombined in the different types of SCCs, showing that tumor heterogeneity did not arise from different levels of oncogene expression or recombination (Figures S1J–S1L). To assess whether Lgr5-derived mixed tumors arise from a clonal event, we induced mice with a lower dose of TAM (1 mg), which strongly decreased the number of tumors per mouse (three versus 20) and thereby the chance that two tumor-initiating clones fused together into a single tumor mass. Despite the reduction of the number of tumors, these mice presented a similar proportion of mixed tumors (Figures S2A–S2D). Using multicolor confetti reporter mice, tumors labeled with one of the four colors contained both Epcam+ and Epcam− labeled cells expressing the same fluorescent protein (Figures S2E and S2F), further supporting that a single tumor-initiating cell gave rise to a mixed tumor. Altogether, these data demonstrate that Kras^{G12D} expression and p53 deletion in HF SCs and their progeny induce SCCs that undergo spontaneous EMT and indicate that the cellular origin of cancer dictates EMT in skin tumors.

We then assessed whether EMT is a progressive process that arises during tumor progression or whether EMT occurs at the early step of tumorigenesis, by analyzing the skin of the mice before the appearance of macroscopically visible tumors. Small microscopic Lgr5-derived tumors were already composed of K14+ and K14-negative cells (Figures S2G and S2H). In addition, the proportion of Epcam+ cells in Lgr5-derived SCCs did not correlate with their size (Figure S2I), further demonstrating that EMT can occur during the early step of tumorigenesis, as it has been recently shown in pancreatic tumors (Rhim et al., 2012).

Intrinsic Priming of HF to Undergo EMT Promoting Clonogenic and Metastatic Potential

To define whether in the absence of their natural environment and surrounding stromal cells, tumor cells are still biased to undergo EMT depending on their cellular origin, we assessed the potential of Epcam+ TECs to undergo EMT in transplantation assays. To avoid the influence of the tumor microenvironment, we transplanted freshly FACS purified tumor cells with Matrigel subcutaneously into immunodeficient mice and assessed their ability to reform secondary tumors that recapitulate the histology and heterogeneity of the primary tumors (Beck and Blanpain, 2013) (Figure 2A). Limiting dilution analyses of transplanted Epcam+ TECs from K14 and Lgr5-derived tumors showed that both TECs presented similar tumor propagating frequency irrespective of their cell of origin (Figure 2B). Transplantation of a single tumor Epcam+ TEC or their progeny gave rise to mixed tumors containing TECs and TMCs, showing their ability to recapitulate the histology of the tumor of origin at the clonal level (Figures S3A–S3L). The histology and the proportion of Epcam+ TECs and Epcam− TMCs from K14 and Lgr5 tumors were very similar to the histology of the primary tumors, with K14CreER mice giving rise preferentially to well-differentiated tumors containing high proportions of Epcam+ TECs, whereas Lgr5-derived tumors were mostly mixed or mesenchymal (Figures 2C–2G). These data indicate that the cancer cell of origin influences the intrinsic ability of tumor-initiating cells to undergo EMT.

Overexpression of EMT transcription factors (TFs) in cancer cell lines promotes tumor renewal capacities in vitro and their ability to form secondary tumors upon transplantation into immunodeficient mice (Puisieux et al., 2014), which suggested that EMT promotes tumor stemness. To determine whether naturally occurring EMT in primary skin tumors is associated with tumor stemness, we assessed TECs and TMCs clonogenic potential in vitro and in vivo. The in vitro colony forming efficiency and total cell output were higher in Epcam− TMCs as compared to Epcam+ TECs (Figures S3M–S3T), showing that spontaneous EMT in SCCs is associated with increased in vitro clonogenicity. Transplantation experiments showed that Epcam− TMCs were more efficient at forming secondary tumors (Figure 2B), although these secondary tumors were exclusively composed of mesenchymal cells, showing that EMT cells, although presenting enhanced renewal cannot revert back to an epithelial state following subcutaneous transplantation (Figures 2F and 2G).

To assess whether EMT increases the metastatic potential of primary skin tumors, we injected intravenously TECs derived from K14 tumors and TECs and TMCs coming from Lgr5 tumors and assessed the number of metastasis 4 weeks later. The number of metastasis was much higher in mice injected with
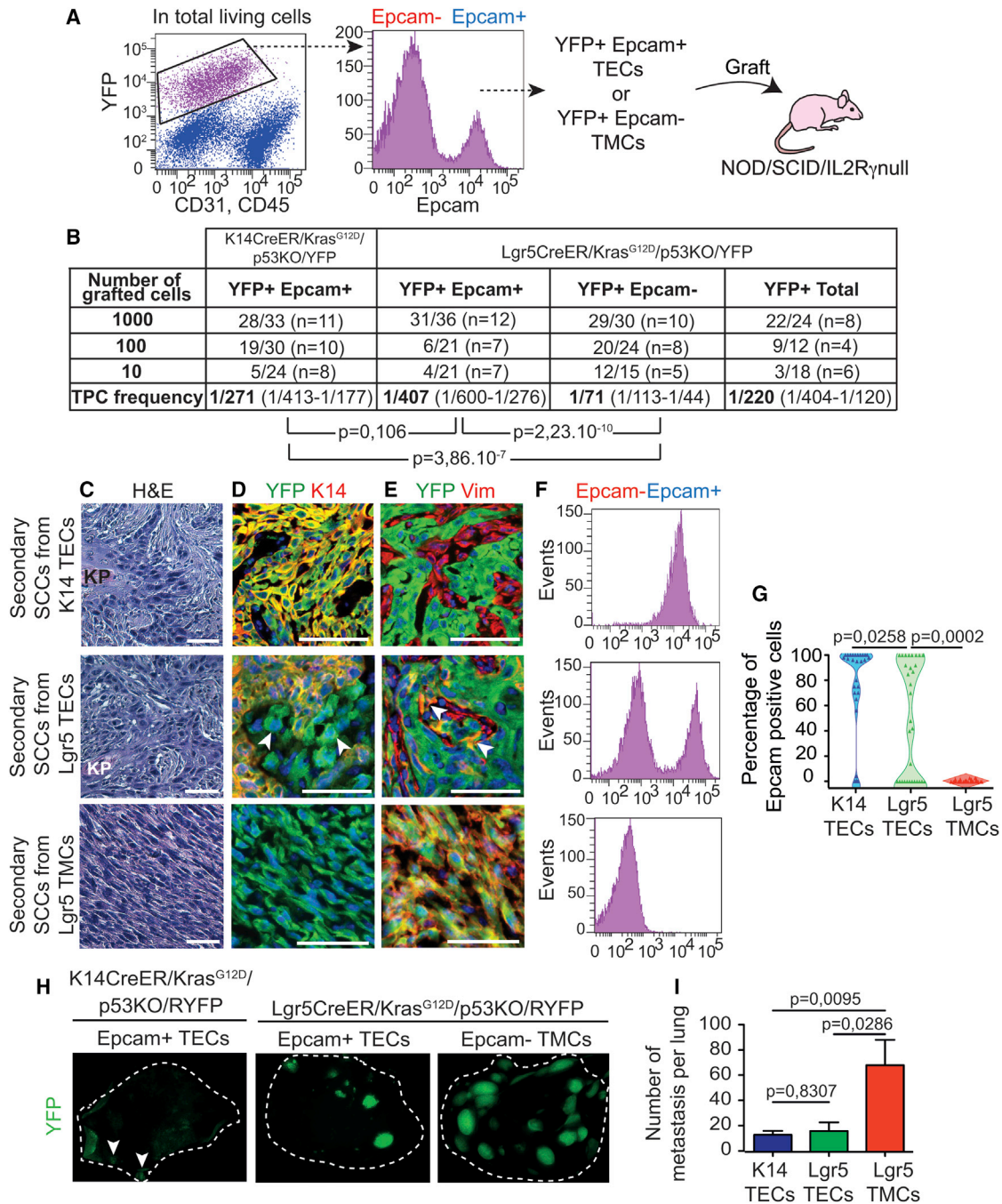
Figure 2. Intrinsic Priming of HF-Derived TECs to Undergo EMT

(A) Scheme representing the strategy of FACS isolation of YFP⁺ Epcam⁺ TECs and YFP⁺ Epcam⁻ TMCs followed by their transplantation into NOD/SCID/Il2Rγ-null mice.

(B) Table summarizing the frequency of secondary tumors observed after transplantation of limiting dilution of YFP⁺ TECs and TMCs into NOD/SCID/Il2Rγ-null mice and the estimation of tumor propagating cells (TPC) frequency for each population. Chi2 test was used for statistical analysis.

(C–E) H&E (C) and immunostaining of YFP and Keratin 14 (K14) (D) or Vimentin (E) in the different secondary tumors.

(F and G) FACS profile (F) and quantification of the percentage of Epcam (G) in the secondary tumors arising from the different TEC and TMC populations (n = 11, n = 12, n = 10, respectively). Scale bars, 50 μm.

(H and I) Macroscopic examination (H) and quantification (I) of YFP+ lung metastases following tail vein injection of 10,000 YFP+ K14 Epcam+ TECs, Lgr5 Epcam+ TECs, or Lgr5 Epcam– TMCs into immunodeficient mice (n =6 independent replicates in each conditions). Histogram represents mean ± SEM in (I).

TMCs compared to TECs (Figures 2H and 2I), demonstrating the greater metastatic potential of skin tumor cells that have undergone EMT.

Altogether these data show that HF-derived tumors are intrinsically primed to undergo EMT and EMT is associated with increased clonogenicity, tumor propagation, and stemness as well as a higher capacity to give rise to metastasis, demonstrating the functional importance of the cancer cell of origin in primary skin SCCs.

Transcriptional Priming of EMT Genes in HF Lineages

To define the mechanisms that promote EMT in primary skin tumors, we first established the transcriptional signature of TECs and TMCs in vivo. To this end, we performed microarray analysis of FACS-isolated YFP$^+$ Epcam$^+$ and Epcam$^-$ tumor cells arising from IFE and HF lineages. Gene ontology of the genome-wide transcriptional analysis confirmed by qRT-PCR and immunostaining showed that K14 and Lgr5 derived Epcam$^+$ TECs were enriched for transcripts regulating the epithelial state, including epidermal markers such as K14, K6, K1, and many TFs known to promote epithelial adhesion, differentiation, and stratification such as *p63* (Mills et al., 1999; Yang et al., 1999), *Ovol* (Lee et al., 2014; Watanabe et al., 2014), *Grhl* (Cieply et al., 2013; Hopkin et al., 2012; Xiang et al., 2012), *Cebpa* (Lopez et al., 2009), and *Klf5* (Kenchegowda et al., 2011) TFs, *Esrp* splicing factors that promote epithelial differentiation and inhibit EMT (Warzecha et al., 2010) as well as different cancer SC markers of well-differentiated SCCs such as *Sox2*, *Vegfa*, and *CD133* (Beck et al., 2011; Boumahdi et al., 2014) (Figures 3A, 3B, and S4A).

In contrast, TMCs were strongly enriched in secreted proteins including components of extracellular matrix (ECM), cell adhesion, ligands, and inhibitors of developmental signaling pathways, regulators of angiogenesis, and various types of mesenchymal collagens (Figure 3C). RT-PCR and immunostaining confirmed the preferential expression of classical EMT markers (Nieto et al., 2016) such as EMT-related TFs *Snai1*, *Zeb1/2*, *Twist1*, and *Prrx1*, EMT-related cytoskeleton (*Vimentin*) and adhesion molecules (*Cdh2/N-cadherin*, *Cadherin 11*), and specific ECM genes such as *Col3a1* and *Fn1* (Figures 3D and S4B).

To assess whether the gene expression in the cancer cell of origin influences the type of tumors that is formed following oncogenic transformation, we performed transcriptional profiling of normal IFE/infundibulum cells (Lgr5-GFP negative, α6HiCD34$^-$) and Lgr5-GFP$^+$ HF cells and compared the genes differentially expressed between normal IFE and HF cells with the genes preferentially expressed in TECs and TMCs they give rise to. Interestingly, 29% of the of genes upregulated in TECs (414/1442) were already upregulated at the mRNA level in IFE compared to HF (Figure 3E). Likewise, 27% of genes upregulated in Epcam$^-$ versus Epcam$^+$ tumor cells (315/1148) were already upregulated at the mRNA level in HF versus IFE (Figure 3F). Gene set enrichment analysis (GSEA), a bioinformatic approach that takes into account all genes and their level of expression, showed a very strong enrichment (normalized enrichment score [NES] >5) of IFE genes within the TEC signature and of HF genes within TMC signature (Figures S4C and S4D), further supporting the notion that transcriptional priming influences the ability of the cancer cell of origin to undergo EMT during tumorigenesis.

The genes transcriptionally primed in IFE lineage and associated with well-differentiated tumors comprised well-known transcription regulators of epidermal differentiation such as *Grhl1/3*, *Cebpa*, *Klf5*, *Ovol1*, and *Pou3f1* (Cieply et al., 2013; Hopkin et al., 2012; Kenchegowda et al., 2011; Lee et al., 2014; Lopez et al., 2009; Watanabe et al., 2014; Xiang et al., 2012), as well as genes associated with epithelial adhesion and epidermal differentiation such as *Klk5, 8, 10, 11, Sprr1a*, or *Tgm3* (Figure 3G). In contrast, the genes primed in HF lineages and that are associated with EMT included well-known HF markers such as *Ltbp2*, *Grem1*, *Flstl1*, *S100A4, Nfatc1, Tbx1, Tcf4, Tcf7l1*, and *Ctgf* (Chen et al., 2012; Horsley et al., 2008; Morris et al., 2004; Nguyen et al., 2009; Tumbar et al., 2004) and mesenchymal genes such as *Col5a2*, *Col6a1*, *Fn1*, and *MMP11* (Figure 3H).

Chromatin Landscape Remodeling during Skin Tumorigenesis

We next defined more globally the changes in the chromatin landscape that occur during tumorigenesis and EMT and assessed whether and how the cancer cell of origin is epigenetically primed to give rise to different tumor phenotypes. To this end, we performed Assay for Tansposase-Accessible Chromatin sequencing (ATAC-seq), a technique that allows the mapping of the open chromatin regions with extremely high definition and with a very low amount of cells (Buenrostro et al., 2013), on FACS-isolated HF and IFE and their respective tumor cell populations, allowing to define the open chromatin regions and the TFs associated with the remodeling of these chromatin regions during tumorigenesis and EMT (Figure 4 and Table S1A). We first defined the chromatin remodeling associated with tumorigenesis, by assessing the chromatin regions (ATAC-seq peaks) that are changed by more than 3-fold, a stringent threshold, between the cell of origin and the respective tumor populations. We identified more open chromatin regions in 477 genes that are upregulated during tumorigenesis across all the different tumor cell populations analyzed (K14 TECs, Lgr5 TECs, Lgr5 TMCs) (Figure 4A; Table S1A), which represent the common epigenetic and transcriptional changes associated with tumor initiation irrespective of the cancer cell of origin and EMT. These genes included ligands of the EGFR pathway (*Areg*, *Ereg*) and TFs known to relay the activation of the Ras/MAPK pathway (*Fos/Fosb*, *Fosl1*, *Nfe2l2*, *Ets1*) and other TFs promoting tumor stemness and invasion (*Twist1*, *Hmga2*, *Prrx1*) (Beck et al., 2015; Copley et al., 2013; Ocaña et al., 2012) (Figures 4B and 4C). Interestingly, the chromatin regions within some of the EMT genes, such as *Snai1* and *Zeb2*, were already opened in Epcam$^+$ tumor cells despite the lack of protein expression (Figures 4D and 4E), suggesting that the EMT program is epigenetically primed in TECs. Motif enrichment analysis of the chromatin regions that opened during tumorigenesis revealed a strong enrichment for the binding site of TFs such as Jun/AP1 (65%), Ets1 (37%), Runx (29%), Nf-kb (22%), and TEAD (25%) (Figure 4F).

Epigenetic Priming of the Cancer Cell of Origin to Undergo EMT

To define the chromatin remodeling that occurred during EMT, we assessed the chromatin regions that were upregulated or downregulated by more than 3-fold between TECs and TMCs from Lgr5-derived tumors (Figures 5A and 5B). GSEA analysis
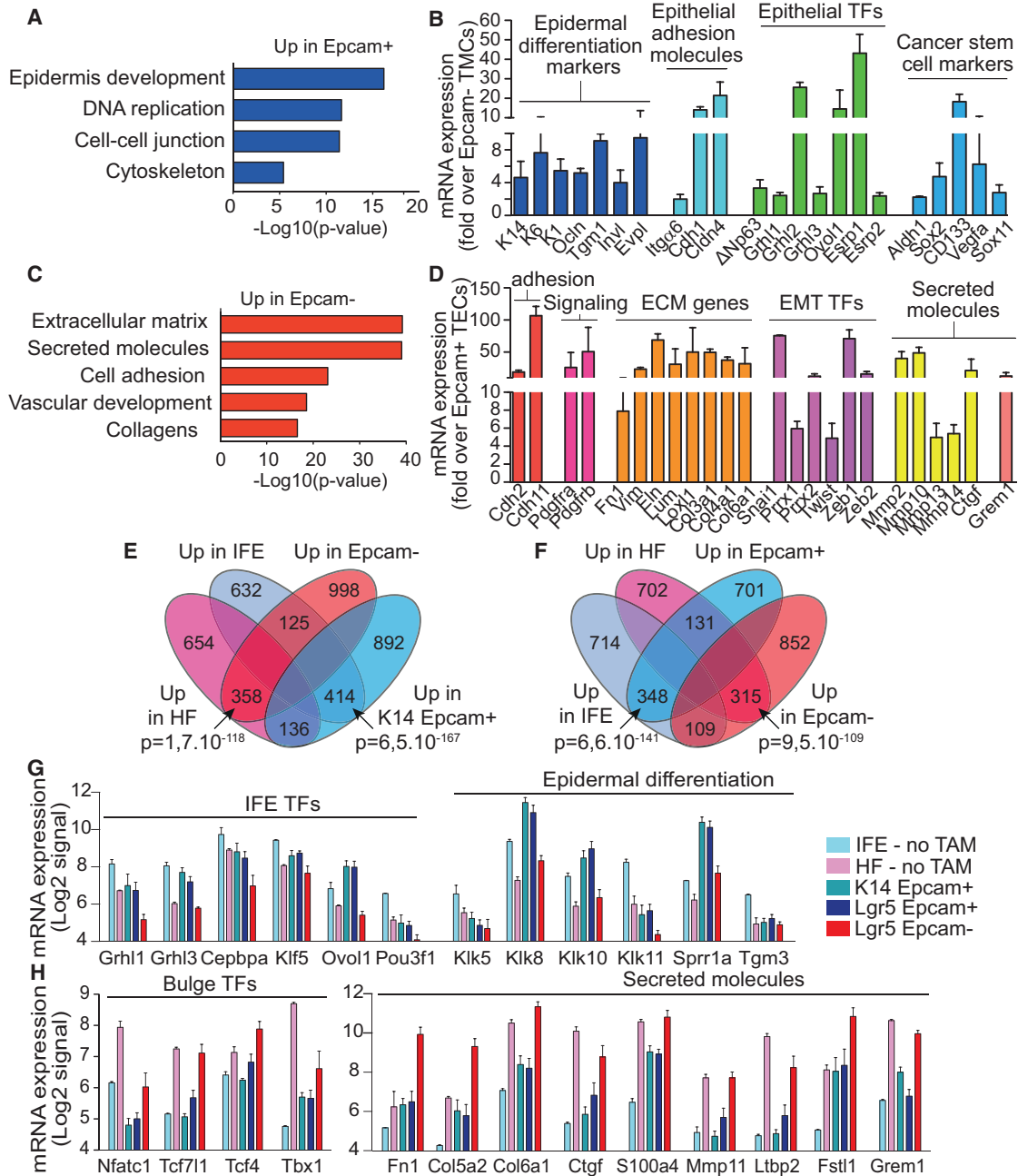
Figure 3. Transcriptional Priming of the Cancer Cell of Origin to Undergo EMT

(A) Gene ontology (GO) analysis of genes upregulated >1.5-fold in TECs compared to TMCs (n = 4).

(B) qRT-PCR of markers upregulated in TECs as compared to TMCs (data are normalized using housekeeping gene TBP, n = 3). Histogram represents mean ± SEM.

(C) GO analysis of genes upregulated >1.5-fold in TMCs compared to TECs (n = 4).

(D) qRT-PCR showing the genes upregulated in TMCs as compared to TECs (n = 4). Histogram represents mean ± SEM.

(E) Venn diagram showing the overlap between the genes upregulated in IFE and in K14-derived Epcam+ TECs.

(F) Venn diagram showing the overlap between the genes upregulated in HF and in Epcam− TMCs.

(G and H) mRNA expression measured by microarray analysis (Log2 signal) of selected genes in FACS-isolated IFE and HF cells and in K14 TECs and Lgr5 TECs and TMCs, showing the transcriptional priming of TEC genes in IFE (G) and the transcriptional priming of TMC genes in HF cells (H) (n = 4). Histogram represents mean ± SEM.
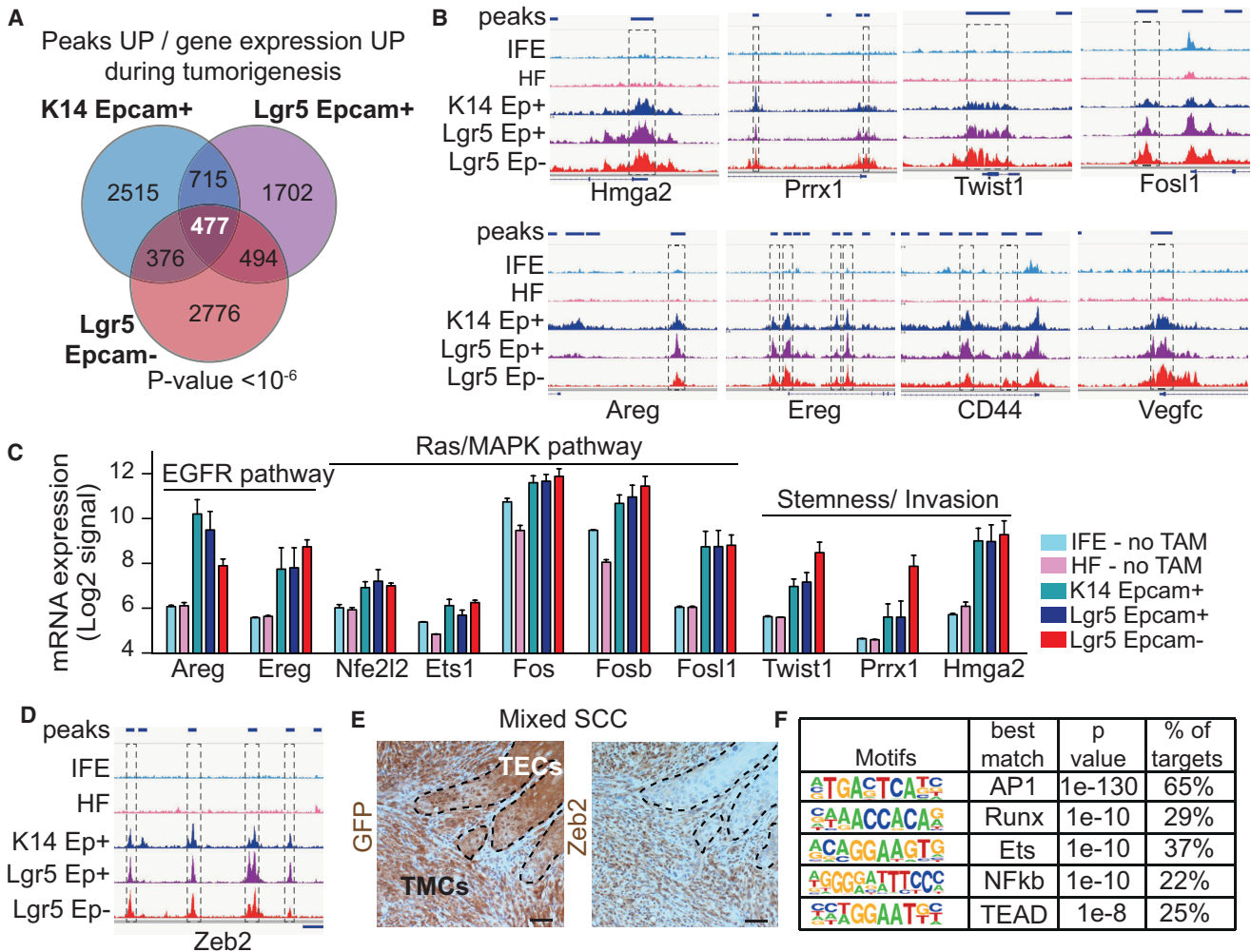
Figure 4. Chromatin Landscape Remodeling during Skin Tumorigenesis

(A) Venn diagram showing the overlap between the genes presenting an ATAC-seq peak upregulated associated with gene expression upregulated in the different populations of tumor cells.

(B) Examples of ATAC-seq profiles of IFE, HF, K14 TECs, and Lgr5 TECs and TMCs showing the appearance of open chromatin regions during tumorigenesis in selected genes upregulated in all tumor cell populations.

(C) mRNA expression of genes upregulated during tumorigenesis measured by microarray analysis (Log2 signal) in FACS-isolated IFE and Lgr5-GFP HF cells and in K14 TECs and Lgr5 TECs and TMCs. Histogram represents mean ± SEM.

(D and E) ATAC-seq profiles of IFE, HF, K14 TECs, and Lgr5 TECs and TMCs showing the opening of chromatin region in Zeb2 in TECs (D), despite the low level of mRNA and the absence of protein expression (E) of Zeb2 in TECs. Scale bars, 50 μm.

(F) Enriched TF motifs found in the ATAC-seq peaks commonly upregulated during tumorigenesis. Scale bars in ATAC-seq represent 2 kb.

showed that the opening of the chromatin was mainly associated with gene activation while chromatin closing was associated with gene repression during EMT (Figures S5A and S5B). To get further insights into the gene regulatory network (GRN) that controls EMT in primary skin tumors, we searched the TF motifs enriched in the chromatin regions that are opened or closed during EMT. The motifs with the highest statistical significance upregulated during EMT and positively associated with gene expression in TMCs were Jun/AP1 (42%), NF1 (45%), Ets1 (10%), bHLH TFs (20%–45%), Nfatc (27%), and Smad2 (37%) (Figure 5C). TFs binding these motifs (e.g., Runx1/2, Nfatc1/2, Twist1/2, Tcf4) were upregulated in Epcam⁻ TMCs (Figure S5C; Table S1B). The same core of TFs including Jun/AP1 (54%), NF1

(48%), Ets1 (29%) was also enriched in the more open chromatin regions in Epcam⁺ TECs (Figure 5D). In addition to this core of TFs, a different set of specific TF motifs including p63 (34%), Grhl (43%), Klf4/5 (18%), Cepba (20%), or Sox2 (25%) was highly enriched in the more open chromatin regions in Epcam⁺ TECs (Figures 5D and S5D; Table S1C). While Zeb1 motif was not particularly enriched in chromatin regions of the genes that were upregulated in TMCs, Zeb1 motif was strongly enriched in chromatin regions that become closed during EMT, supporting the notion that Zeb1 mainly acts as a transcriptional repressor (Eger et al., 2005). Smad2 motif was also strongly enriched in chromatin peaks that are closed in TMCs (42% of the peaks), suggesting that transforming growth factor β
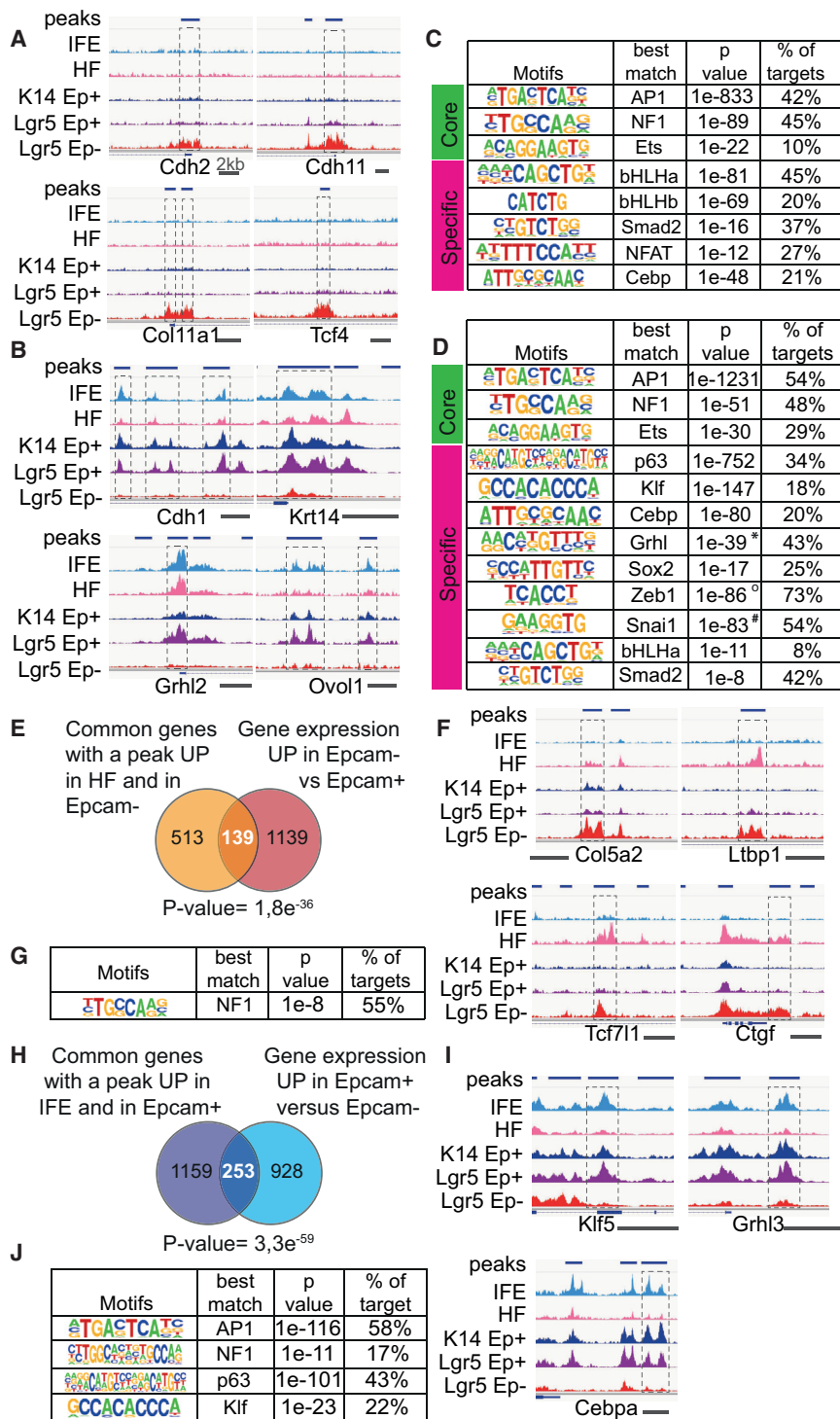
Figure 5. Chromatin Landscape Remodeling during EMT and Epigenetic Priming of the Cancer Cell of Origin

(A and B) Examples of ATAC-seq profiles of genes showing opening of the chromatin regions in Lgr5 TMCs (A) and TECs (B).

(C and D) TF motifs enriched in the open chromatin regions in TMCs (C) or TECs (D) using known motifs. *De novo motifs; ° and #, search using JASPAR motif matrix.

(E) Venn diagram of the genes showing the overlap between the genes with ATAC-seq peak upregulated in HF and in TMCs and the genes upregulated in TMCs versus TECs.

(F) ATAC-seq profiles of IFE, HF, K14 TECs, and Lgr5 TECs and TMCs showing the opening of chromatin region in epigenetically primed genes in HF.

(G) TF motif found in the ATAC-seq peaks upregulated during EMT and HF and associated with gene upregulation in TMCs.

(H) Venn diagram showing the overlap between the genes with ATAC-seq peak upregulated in IFE and in K14 TECs and genes that are upregulated in TECs versus TMCs.

(I) ATAC-seq profiles of IFE, HF, K14 TECs, and Lgr5 TECs and TMCs showing the opening of chromatin region in epigenetically primed genes in IFE.

(J) TF motifs enriched in the ATAC-seq peaks upregulated in TECs and IFE and associated with gene upregulation in Epcam⁺ TECs. Scale bars in ATAC-seq represent 2 kb.

C

Motifs	best match	p value	% of targets
Core — AP1	AP1	1e-833	42%
NF1	NF1	1e-89	45%
Ets	Ets	1e-22	10%
Specific — bHLHa	bHLHa	1e-81	45%
bHLHb	bHLHb	1e-69	20%
Smad2	Smad2	1e-16	37%
NFAT	NFAT	1e-12	27%
Cebp	Cebp	1e-48	21%

D

Motifs	best match	p value	% of targets
Core	AP1	1e-1231	54%
	NF1	1e-51	48%
	Ets	1e-30	29%
Specific	p63	1e-752	34%
	Klf	1e-147	18%
	Cebp	1e-80	20%
	Grhl	1e-39 *	43%
	Sox2	1e-17	25%
	Zeb1	1e-86 °	73%
	Snai1	1e-83 #	54%
	bHLHa	1e-11	8%
	Smad2	1e-8	42%

E Common genes with a peak UP in HF and in Epcam- / Gene expression UP in Epcam- vs Epcam+

513 | 139 | 1139

P-value= 1,8e⁻³⁶

G

Motifs	best match	p value	% of targets
NF1	NF1	1e-8	55%

H Common genes with a peak UP in IFE and in Epcam+ / Gene expression UP in Epcam+ versus Epcam-

1159 | 253 | 928

P-value= 3,3e⁻⁵⁹

J

Motifs	best match	p value	% of target
AP1	AP1	1e-116	58%
NF1	NF1	1e-11	17%
p63	p63	1e-101	43%
Klf	Klf	1e-23	22%

already presented more open chromatin regions in HF, suggesting that these genes are epigenetically primed in HF to facilitate EMT during tumorigenesis (Figures 5E, S5E, and S5F). These genes including *Tcf7l1*, *Ltbp1*, and *Zeb1* were enriched for NF1 binding site (Figures 5F and 5G), some of which share the same active enhancers in HFs and TMCs (Figure S5G). About half (45%) of the epigenetically primed genes were already upregulated in HF cells (Figure S5F; Table S1D). These data indicate the chromatin landscape of HF primes these cells to undergo EMT during tumorigenesis. We next analyzed whether the chromatin landscape of the IFE primes these cells to give rise to well-differentiated tumors (Figure S5H). Interestingly, 253 genes transcriptionally upregulated in Epcam⁺ TECs presented more open chromatin regions in IFE (Figures 5H and 5I), among which 112 genes were already transcriptionally upregulated in IFE (Figure S5I; Table S1E). The common open chromatin regions between IFE cells and Epcam⁺ TECs included the regulatory regions of the key TFs promoting epidermal differentiation such as *p63*, *Klf5*, *Grhl1/3*, or *Cepba* (Figures 5I and S5J). These commonly upregulated chromatin

(TGF-β)/Smad2 axis acts both as transcriptional activator and repressor during EMT (Figure 5D).

To assess whether the epigenetic landscape of the cancer cell of origin promotes or restricts gene expression and EMT in skin tumors, we compared the chromatin landscape of the cancer cell of origin to the tumor cells they derived. Interestingly, we found that 139 genes transcriptionally upregulated during EMT

regions between IFE and Epcam$^+$ TECs were highly enriched for Jun/AP1 (58%), p63 (43%), and Klf (22%) binding sites (Figure 5J), suggesting that p63 and Klf TFs contribute to the epigenetic priming of IFE cells to give rise to well-differentiated tumors upon oncogenic transformation.

Activator and Repressor Functions of Epithelial and Mesenchymal TFs

To functionally challenge the bioinformatic predictions of the GRNs that positively and negatively control EMT in primary skin SCCs (Figures 6A, 6B, S6, and S7), we performed short hairpin RNA (shRNA) knockdown (KD) of TFs predicted to control the GRNs associated with EMT in vivo and assessed the impact of their KD on the regulation of epithelial and mesenchymal gene expression. FACS-isolated Epcam$^+$ and Epcam$^-$ cells were cultured on irradiated 3T3 feeder layers, and the tumor cells were infected with lentiviruses expressing shRNA against *p63*, *Klf5*, *Twist1*, *Zeb1*, or *Snai1*, the most statistically significant TF motifs found in the open or close chromatin regions during EMT (Figures 6C and 6D).

Consistent with the high enrichment of Klf5 and p63 motifs in the open chromatin regions of the genes associated with TEC state, shRNA against *p63* or *Klf5* in TECs resulted in the downregulation of key epidermal TFs (*Grhl2*, *Cepba*, and *p63*) and epithelial markers (*Ecadh*, *K5*) that presented p63 and Klf5 motifs in their open chromatin regions, supporting the notion that p63 and Klf5 act as transcriptional activators of gene expression (Figure 6C). The EMT genes upregulated following *p63* and *Klf5* KD such as Zeb were not enriched in p63 and Klf5 motifs in their open chromatin regions, suggesting that this effect was indirect (Figure 6C). In contrast to the transcriptional activator function of the key epithelial TFs, the classical EMT TFs Zeb1, Snai1, and Twist1 mainly act as transcriptional repressors, as suggested by the presence of their binding sites in the chromatin regions that are closed during EMT, and the upregulation of key epidermal TFs such as *p63*, *Cepba*, and *Grhl2* and epithelial genes such as *Ecadh* and *K5* following their shRNA KD in vitro (Figure 6D). In addition to repressing gene expression, these EMT TFs could also positively regulate the expression of some mesenchymal genes (e.g., Cdh11 by Zeb1). Altogether, the consequences of shRNA KD of several key TFs predicted to regulate the expression of genes during EMT are consistent with the bioinformatic prediction and support the notion that these key epithelial TFs act mainly as transcriptional activators, whereas the classical EMT TFs act mainly as transcriptional repressors.

TGF-β-induced EMT is the most commonly used method to promote EMT in cancer cells (Moustakas and Heldin, 2014). To further challenge the bioinformatic prediction of the GRN associated with EMT, we assessed how p-Smad2 activation mediated by TGF-β signaling regulates the expression of the genes containing Smad2 binding sites in the chromatin regions that are remodeled during EMT. RNA-seq performed 48 hr following the addition of TGF-β to Epcam$^+$ Lgr5-derived TECs showed that 20% of the upregulated genes and 30% of the downregulated genes that contained chromatin regions with Smad2 motifs remodeled during EMT were differentially regulated by TGF-β treatment (Figures 6E and 6F), showing that TGF-β/Smad2 axis activates and represses gene expression during EMT as predicted by our GRN models.

ΔNp63 Primes the Cancer Cell of Origin toward Well-Differentiated Tumors

Our bioinformatic analysis suggests that p63 regulates the epigenetic and transcriptional priming of IFE cancer cell of origin toward well-differentiated SCCs. Immunostaining for p63 in the different SCC subtypes showed that p63 was only expressed in TECs and not in TMCs, consistent with this possibility (Figure 7A). To test this hypothesis, we generated Lgr5CreER/KRas^{G12D}/p53$^{fl/fl}$/Rosa-ΔNp63-IRES-GFP mice (Figure 7B), allowing constitutive expression of ΔNp63 together with KRasG12D activation and p53 deletion in HF lineages to assess whether the sustained expression of p63 restricts EMT in HF-derived tumors. Whereas the number of tumors that formed in homozygous ΔNp63-IRES-GFP mice was unchanged (Figure 7C), the proportion of well-differentiated SCCs was strongly increased in Lgr5-derived tumors that expressed ΔNp63 (Figures 7D and 7E).

To further define the molecular mechanisms by which ΔNp63 promotes the well-differentiated tumor phenotypes, we performed transcriptional profiling of FACS-isolated GFP$^+$ Epcam$^-$ tumor cells from Lgr5CreER/KRas^{G12D}/p53$^{fl/fl}$/Rosa ΔNp63-IRES-GFP-induced mice. We found that the sustained expression of ΔNp63 induced the upregulation of 566 genes in Epcam$^-$ cells, among which 329 genes (58%) belong the TEC signature (p < 10^{-16}) (Figure 7F; Table S1F). GSEA analysis further demonstrated the major enrichment of genes of the TEC signature in Epcam$^-$ cells overexpressing ΔNp63 (Figure 7G). Many of these genes contained p63 motifs in the open chromatin regions of Epcam$^+$ TECs and IFE cells, supporting the notion that p63 directly regulates their expression during tumorigenesis (Figure 7H).

To functionally assess whether p63 restricts EMT induced by extrinsic cues, we assessed the ability of TGF-β to induce EMT in K14 and Lgr5-derived TECs overexpressing ΔNp63. K14-derived TECs were much more resistant to TGF-β-induced EMT as compared to Lgr5-derived TECs (Figure 7I), further demonstrating the intrinsic priming of Lgr5-derived TECs toward EMT as compared to IFE-derived TECs. Interestingly, Lgr5 TECs overexpressing p63 were also much more resistant to TGF-β-induced EMT as compared to Lgr5 TECs that did not overexpress p63 (Figure 7I), showing that p63 opposes TGF-β-induced EMT.

These data demonstrate that ΔNp63 acts functionally and molecularly as a master regulator of the TEC fate in vivo and primes the IFE cancer cell of origin toward well-differentiated SCCs.

DISCUSSION

Here, using lineage-tracing experiments allowing the expression of the same oncogenic hits in different epidermal lineages, we showed for the first time that cancer cell of origin controls EMT in skin SCCs. The transplantation of FACS-isolated TECs in the absence of their underlying microenvironment lead to the same biases to undergo EMT, suggesting that intrinsic factors promote EMT in oncogene-targeted HF cells. Likewise, HF-derived TECs are much more sensitive to TGF-β-induced EMT, further demonstrating that intrinsic factors and higher propensity to respond to TGF-β signaling promote EMT in HF-derived tumors.
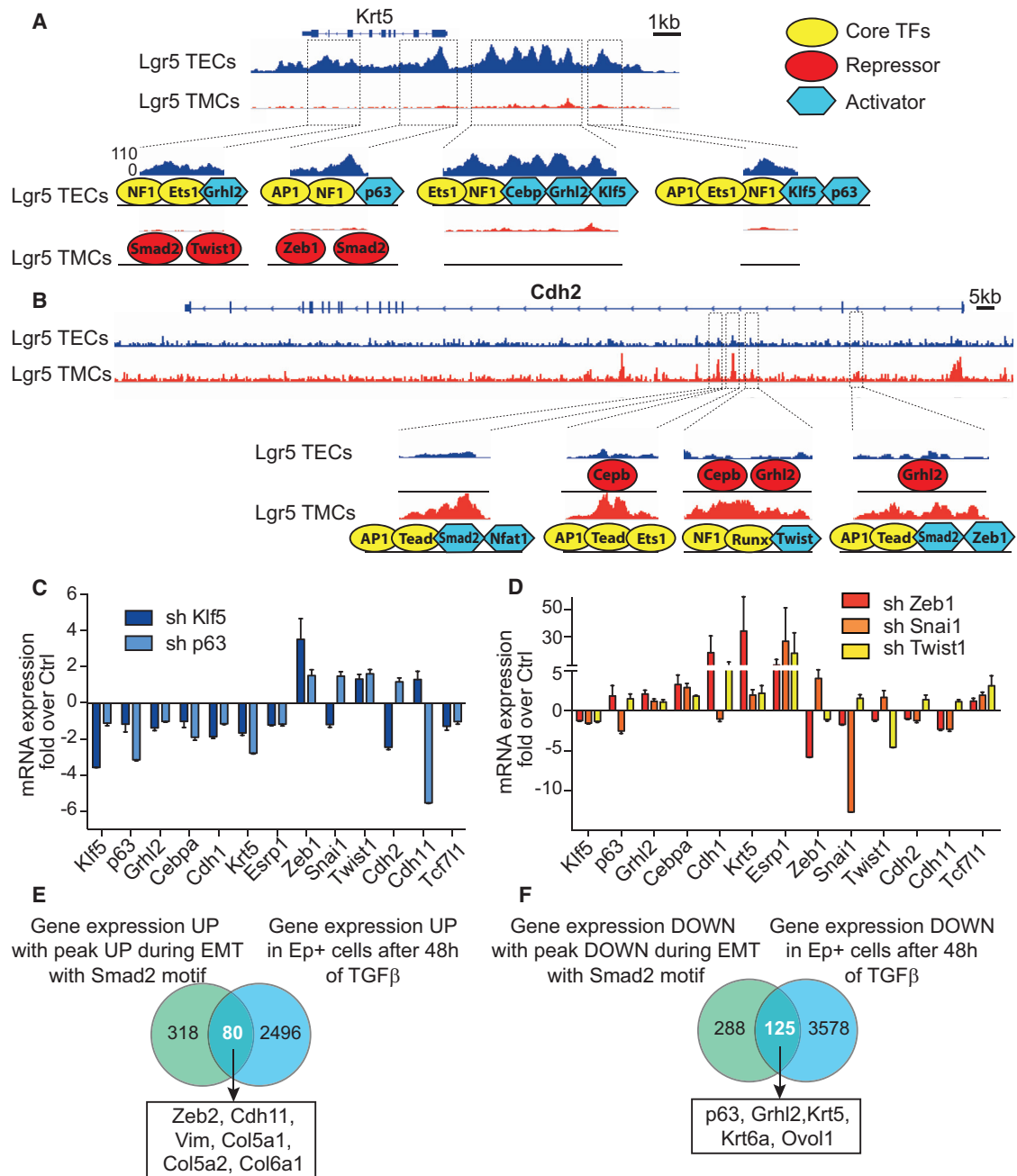
Figure 6. Activator and Repressor Functions of Epithelial and Mesenchymal TFs during EMT

(A and B) Representation of chromatin remodeling and their associated TFs in Krt5 (A) and Cdh2 (B) during EMT.

(C and D) Epithelial and mesenchymal gene expression after shRNA knockdown of *Klf5* and *p63* TECs (C) and *Zeb1*, *Snai1*, and *Twist1* in TMCs (D). Histogram represents mean ± SEM.

(E) Venn diagram showing the overlap between the genes upregulated in Epcam⁻ cells and containing a Smad2 motif in their open chromatin region during EMT and the genes upregulated by more than 1.5-fold in TECs 48 hr after TGF-β addition.

(F) Venn diagram showing the overlap between the genes downregulated in TMCs and containing a Smad2 motif in their close chromatin region during EMT and the genes downregulated by more than 1.5-fold in TECs 48 hr after TGF-β addition.

Our genome-wide transcriptional analysis of the cancer cell of origin and their corresponding tumor cells during skin tumorigenesis allows defining the molecular determinants that regulate EMT in primary tumors in vivo. In addition to these novel in vivo EMT transcriptional signatures, we unravel for the first time the changes in the chromatin landscape occurring during cancer initiation and EMT in primary tumors in vivo that provide novel insights into the mechanisms by which the cancer cell of origin regulates EMT during tumorigenesis in vivo (Figure S7).
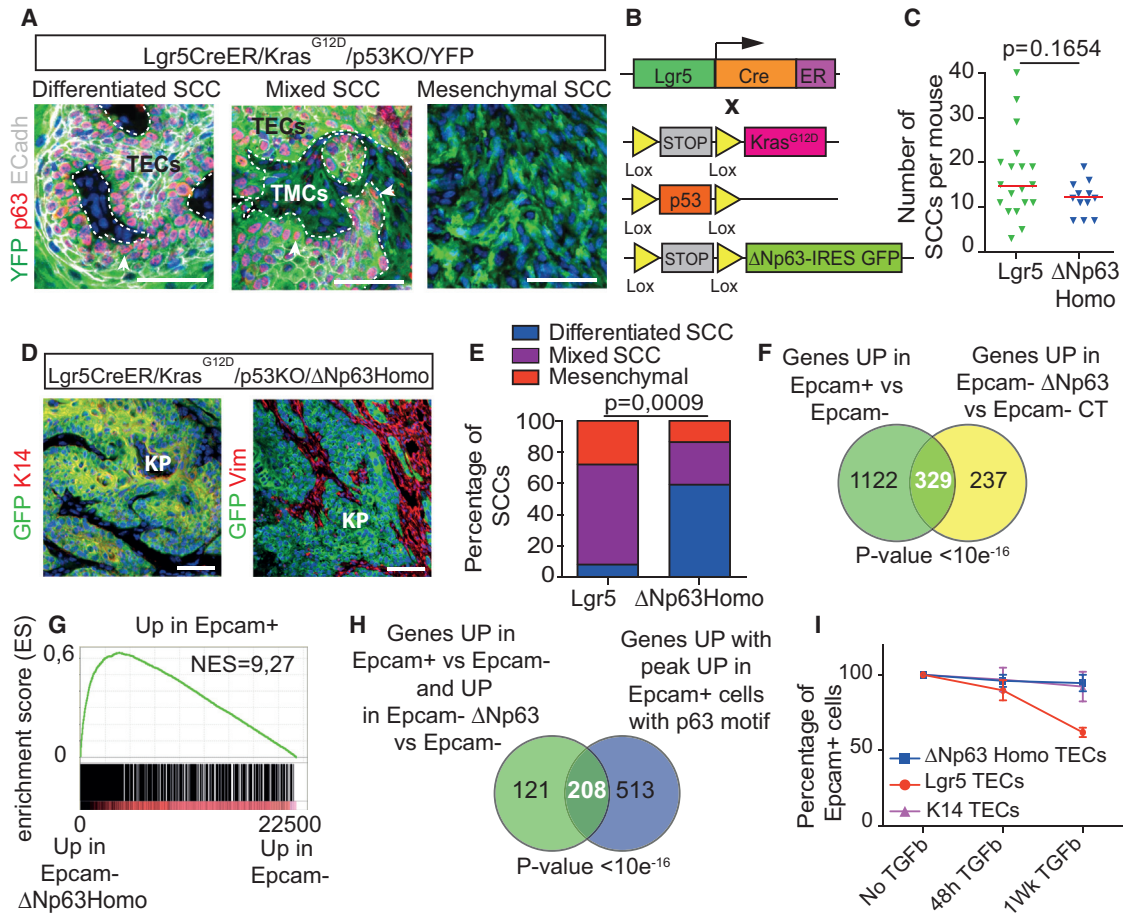
Figure 7. ΔNp63 Overexpression Restricts EMT in Oncogene-Targeted HF Cells

(A) Co-immunostaining for YFP, p63, and Ecadh in the different subtypes of SCCs arising from Lgr5CreER mice. Scale bars, 50 μm.

(B) Genetically engineered mouse models allowing the expression Kras[G12D] as well as p53 deletion together with ΔNp63-IRES-GFP overexpression in HF lineages.

(C) Number of SCCs per mouse in the presence (homozygous for ΔNp63-IRES-GFP) (n = 12) or the absence of ΔNp63 overexpression (n = 19).

(D) Co-immunostaining showing the expression of YFP and K14 and Vimentin in Lgr5CreER/KrasG12D/p53KO/ΔNp63 homozygous skin tumors, showing the promotion of epithelial differentiation in HF-derived tumors upon ΔNp63 overexpression. Scale bars, 50 μm.

(E) Graph showing the proportion of differentiated, mixed, and mesenchymal tumors in Lgr5CreER/KrasG12D/p53KO/ΔNp63 and control Lgr5CreER/KrasG12D/p53KO/YFP mice based on their histology (n = 22 and n = 25, respectively).

(F) Venn diagram showing overlap between the genes upregulated in TMCs after ΔNp63 overexpression and the genes upregulated in TECs.

(G) GSEA analysis of the upregulated genes in TECs with the genes upregulated in TMCs after ΔNp63 overexpression, showing the enrichment of the TEC signature in Epcam⁻ cells overexpressing p63.

(H) Venn diagram showing overlap between genes up in Epcam⁺ TECs versus Epcam⁻ TMCs and up in Epcam⁻ ΔNp63 versus control with the genes up with peak up with a p63 motif.

(I) Graph showing the percentage of Epcam⁺ TECs after 48 hr and 1 week of TGF-β treatment to Epcam⁺ TECs from K14 and Lgr5 with and without p63 overexpression (n > 3, mean ± SEM, n = 9, n = 3, and n = 5 tumors, respectively). Histogram represents mean ± SEM.

Bioinformatic analysis of the chromatin remodeling during tumorigenesis reveals a core of TFs promotes gene expression during tumorigenesis independently of the cell of origin and EMT. The most enriched motif (60%) in these common open chromatin regions of tumor cells is AP1, which corresponds to the binding site of Jun/Fos TFs. Transcriptional analysis revealed that several members of the Jun/Fos family were upregulated in tumor cells as compared to their cell of origin, including *Fosl1*, *Fosb*, *Fos*, and *Junb*, consistent with the well-known functions of *Jun/Fos* family members in relaying transcriptional regulation downstream of oncogenic Ras/MAPK activation (Eferl

and Wagner, 2003). Motifs for Ets, another family of TFs known to relay oncogenic Ras/MAPK signaling in skin tumors (Dittmer, 2015; Yang et al., 2015), and for Runx1, Tead, and Nfκb TFs, which regulate skin tumorigenesis in vivo (Hoi et al., 2010; Zanconato et al., 2015; Zhu et al., 2009), were also highly enriched in the open chromatin of all tumor cells.

In addition to these core TFs, lineage-specific TFs regulate the specificity of the tumor phenotypes and EMT in skin tumors. *P63*, *Klf*, *Grhl*, and *Cepba* are upregulated in TECs, and their binding sites are enriched in the TEC open chromatin regions, suggesting they regulate the GRN that promote squamous differentiation

in oncogene-targeted IFE cells. Klf5 and p63 are the most significant TFs associated with the priming of IFE toward well-differentiated SCCs. *KLF5* is mutated and acts as a genetic driver in lung carcinomas, including lung SCCs (Campbell et al., 2016). Super-enhancer amplification associated with increased *KLF5* expression has been recently found in head and neck SCCs (Zhang et al., 2016), and Klf5 prevents apoptosis induced by TGF-β signaling (David et al., 2016). P63 is the master regulator of epidermal stratification, promotes SC renewal in stratified epithelia and is expressed in different human carcinomas (Melino et al., 2015). Our functional in vitro and in vivo gain- and loss-of-function experiments showed that Klf5 and p63 act as master regulators of the epithelial state and prime the IFE cells into well-differentiated tumors upon oncogenic Ras expression and cooperated with the core TFs such as AP1 and Ets, to positively regulate gene expression in TECs. By promoting the expression of micro-RNAs such as miR-200, which target key EMT TFs (Wellner et al., 2009), p63 and Klf5 also participate to the down-regulation of EMT genes such as Zeb1 (Zhang et al., 2013; Zhao et al., 2016).

During EMT, the core TFs cooperate with EMT-specific TFs including bHLH, Runx, Nfat, and Smad2 TFs, several of which are well known to be preferentially expressed in normal HF SCs and to regulate their function (Blanpain et al., 2004; Morris et al., 2004; Tumbar et al., 2004). Our functional data using shRNA-mediated KD of the well-known canonical EMT TFs confirm that, in contrast to the positive gene regulation mediated by the key epithelial TFs, these EMT TFs mainly act as transcriptional repressors. Our data indicate that the TGF-β/Smad2 axis rapidly activates and represses a large number of genes associated with EMT that present Smad2 binding sites in their open or close chromatin regions in good agreement with the well-known pro-EMT role of TGF-β (Siegel and Massagué, 2003) and the recent data showing that TGF-β-responsive cells mediated cell invasion in skin SCCs (Paniz-Mondolfi et al., 2015).

The remarkable and unexpected similarity in the chromatin and transcriptional landscape between HF lineage and EMT cells suggests that many EMT genes are primed in the HF lineages and facilitate the development of EMT in HF-derived tumors. The EMT primed genes in HF lineages consist of TFs associated with HF stemness and differentiation (Runx1, Nfatc1, Tcf7l1, Tbx1) (Chen et al., 2012; Horsley et al., 2008; Morris et al., 2004; Nguyen et al., 2006; Tumbar et al., 2004), and a great number of secreted molecules promoting TGF-β signaling (Ltbp1, 3) or inhibiting BMP signaling (Grem1, Flstl1), ECM proteins (Col, Postn, Lox), leading to the autocrine or paracrine formation of an EMT prone niche in the HF lineages that promotes EMT in HF oncogene-targeted cells. The transcriptional and epigenetic priming of the cancer cell of origin to undergo EMT does not exclude that part of the changes in gene expression and epigenetic landscape can be also the consequence of regulatory signals arising from the microenvironment. Future studies will be needed to identify the importance and nature of extrinsic signals released in a paracrine or autocrine manner by the tumor cells and their stromal cells that regulate the epigenetic landscape of tumor cells and EMT.

In conclusion, our study demonstrates the functional importance of the cancer cell of origin in regulating EMT and uncovers the molecular mechanisms by which the cancer cell of origin promotes or restricts EMT in primary skin tumors.

STAR★METHODS

Detailed methods are provided in the online version of this paper and include the following:

- KEY RESOURCES TABLE
- CONTACT FOR REAGENT AND RESOURCE SHARING
- EXPERIMENTAL MODEL AND SUBJECT DETAILS
  - Mice
  - Primary cell culture
- METHOD DETAILS
  - KRasG12D p53fl/fl induced skin tumors
  - Monitoring of tumor growth
  - Antibodies
  - Histology and immunostaining
  - Image acquisition
  - FACS Isolation of TECs and TMCs
  - Tumor transplantation assays
  - In vitro TGF-β treatment
  - Virus production, infection and selection
  - RNA and DNA extraction, real-time PCR
  - Microarray analysis
  - ATAC-seq
  - Library preparation and sequencing
  - Alignment and Peak calling
  - Differential Peak analysis
  - Motif analysis
  - GSEA analysis
  - RNA sequencing
- QUANTIFICATION AND STATISTICAL ANALYSIS
  - Estimation of tumor propagating cell frequency
  - Statistics
- DATA AND SOFTWARE AVAILABILITY
- ADDITIONAL RESOURCES

REFERENCES

Anders, S., Pyl, P.T., and Huber, W. (2015). HTSeq—A Python framework to work with high-throughput sequencing data. Bioinformatics *31*, 166–169.

Barker, N., van Es, J.H., Kuipers, J., Kujala, P., van den Born, M., Cozijnsen, M., Haegebarth, A., Korving, J., Begthel, H., Peters, P.J., and Clevers, H. (2007). Identification of stem cells in small intestine and colon by marker gene Lgr5. Nature *449*, 1003–1007.

Beck, B., and Blanpain, C. (2013). Unravelling cancer stem cell potential. Nat. Rev. Cancer *13*, 727–738.

Beck, B., Driessens, G., Goossens, S., Youssef, K.K., Kuchnio, A., Caauwe, A., Sotiropoulou, P.A., Loges, S., Lapouge, G., Candi, A., et al. (2011). A vascular niche and a VEGF-Nrp1 loop regulate the initiation and stemness of skin tumours. Nature *478*, 399–403.

Beck, B., Lapouge, G., Rorive, S., Drogat, B., Desaedelaere, K., Delafaille, S., Dubois, C., Salmon, I., Willekens, K., Marine, J.C., and Blanpain, C. (2015). Different levels of Twist1 regulate skin tumor initiation, stemness, and progression. Cell Stem Cell *16*, 67–79.

Blanpain, C. (2013). Tracing the cellular origin of cancer. Nat. Cell Biol. *15*, 126–134.

Blanpain, C., and Fuchs, E. (2014). Stem cell plasticity. Plasticity of epithelial stem cells in tissue regeneration. Science *344*, 1242281.

Blanpain, C., Lowry, W.E., Geoghegan, A., Polak, L., and Fuchs, E. (2004). Self-renewal, multipotency, and the existence of two cell populations within an epithelial stem cell niche. Cell *118*, 635–648.

Boumahdi, S., Driessens, G., Lapouge, G., Rorive, S., Nassar, D., Le Mercier, M., Delatte, B., Caauwe, A., Lenglez, S., Nkusi, E., et al. (2014). SOX2 controls tumour initiation and cancer stem-cell functions in squamous-cell carcinoma. Nature *511*, 246–250.

Buenrostro, J.D., Giresi, P.G., Zaba, L.C., Chang, H.Y., and Greenleaf, W.J. (2013). Transposition of native chromatin for fast and sensitive epigenomic profiling of open chromatin, DNA-binding proteins and nucleosome position. Nat. Methods *10*, 1213–1218.

Campbell, J.D., Alexandrov, A., Kim, J., Wala, J., Berger, A.H., Pedamallu, C.S., Shukla, S.A., Guo, G., Brooks, A.N., Murray, B.A., et al.; Cancer Genome Atlas Research Network (2016). Distinct patterns of somatic genome alterations in lung adenocarcinomas and squamous cell carcinomas. Nat. Genet. *48*, 607–616.

Chen, T., Heller, E., Beronja, S., Oshimori, N., Stokes, N., and Fuchs, E. (2012). An RNA interference screen uncovers a new molecule in stem cell self-renewal and long-term regeneration. Nature *485*, 104–108.

Cieply, B., Farris, J., Denvir, J., Ford, H.L., and Frisch, S.M. (2013). Epithelial-mesenchymal transition and tumor suppression are controlled by a reciprocal feedback loop between ZEB1 and Grainyhead-like-2. Cancer Res. *73*, 6299–6309.

Copley, M.R., Babovic, S., Benz, C., Knapp, D.J., Beer, P.A., Kent, D.G., Wohrer, S., Treloar, D.Q., Day, C., Rowe, K., et al. (2013). The Lin28b-let-7-Hmga2 axis determines the higher self-renewal potential of fetal haemato-poietic stem cells. Nat. Cell Biol. *15*, 916–925.

David, C.J., Huang, Y.H., Chen, M., Su, J., Zou, Y., Bardeesy, N., Iacobuzio-Donahue, C.A., and Massagué, J. (2016). TGF-β Tumor Suppression through a Lethal EMT. Cell *164*, 1015–1030.

Dittmer, J. (2015). The role of the transcription factor Ets1 in carcinoma. Semin. Cancer Biol. *35*, 20–38.

Eferl, R., and Wagner, E.F. (2003). AP-1: A double-edged sword in tumorigenesis. Nat. Rev. Cancer *3*, 859–868.

Eger, A., Aigner, K., Sonderegger, S., Dampier, B., Oehler, S., Schreiber, M., Berx, G., Cano, A., Beug, H., and Foisner, R. (2005). DeltaEF1 is a transcriptional repressor of E-cadherin and regulates epithelial plasticity in breast cancer cells. Oncogene *24*, 2375–2385.

Heinz, S., Benner, C., Spann, N., Bertolino, E., Lin, Y.C., Laslo, P., Cheng, J.X., Murre, C., Singh, H., and Glass, C.K. (2010). Simple combinations of lineage-determining transcription factors prime cis-regulatory elements required for macrophage and B cell identities. Mol. Cell *38*, 576–589.

Hoi, C.S., Lee, S.E., Lu, S.Y., McDermitt, D.J., Osorio, K.M., Piskun, C.M., Peters, R.M., Paus, R., and Tumbar, T. (2010). Runx1 directly promotes proliferation of hair follicle stem cells and epithelial tumor formation in mouse skin. Mol. Cell. Biol. *30*, 2518–2536.

Hopkin, A.S., Gordon, W., Klein, R.H., Espitia, F., Daily, K., Zeller, M., Baldi, P., and Andersen, B. (2012). GRHL3/GET1 and trithorax group members collaborate to activate the epidermal progenitor differentiation program. PLoS Genet. *8*, e1002829.

Horsley, V., Aliprantis, A.O., Polak, L., Glimcher, L.H., and Fuchs, E. (2008). NFATc1 balances quiescence and proliferation of skin stem cells. Cell *132*, 299–310.

Hu, Y., and Smyth, G.K. (2009). ELDA: Extreme limiting dilution analysis for comparing depleted and enriched populations in stem cell and other assays. J. Immunol. Methods *347*, 70–78.

Jonkers, J., Meuwissen, R., van der Gulden, H., Peterse, H., van der Valk, M., and Berns, A. (2001). Synergistic tumor suppressor activity of BRCA2 and p53 in a conditional mouse model for breast cancer. Nat. Genet. *29*, 418–425.

Kenchegowda, D., Swamynathan, S., Gupta, D., Wan, H., Whitsett, J., and Swamynathan, S.K. (2011). Conditional disruption of mouse Klf5 results in defective eyelids with malformed meibomian glands, abnormal cornea and loss of conjunctival goblet cells. Dev. Biol. *356*, 5–18.

Langmead, B., and Salzberg, S.L. (2012). Fast gapped-read alignment with Bowtie 2. Nat. Methods *9*, 357–359.

Lapouge, G., Youssef, K.K., Vokaer, B., Achouri, Y., Michaux, C., Sotiropoulou, P.A., and Blanpain, C. (2011). Identifying the cellular origin of squamous skin tumors. Proc. Natl. Acad. Sci. USA *108*, 7431–7436.

Lapouge, G., Beck, B., Nassar, D., Dubois, C., Dekoninck, S., and Blanpain, C. (2012). Skin squamous cell carcinoma propagating cells increase with tumour progression and invasiveness. EMBO J. *31*, 4563–4575.

Lee, B., Villarreal-Ponce, A., Fallahi, M., Ovadia, J., Sun, P., Yu, Q.C., Ito, S., Sinha, S., Nie, Q., and Dai, X. (2014). Transcriptional mechanisms link epithelial plasticity to adhesion and differentiation of epidermal progenitor cells. Dev. Cell *29*, 47–58.

Lopez, R.G., Garcia-Silva, S., Moore, S.J., Bereshchenko, O., Martinez-Cruz, A.B., Ermakova, O., Kurz, E., Paramio, J.M., and Nerlov, C. (2009). C/EBPalpha and beta couple interfollicular keratinocyte proliferation arrest to commitment and terminal differentiation. Nat. Cell Biol. *11*, 1181–1190.

Love, M.I., Huber, W., and Anders, S. (2014). Moderated estimation of fold change and dispersion for RNA-seq data with DESeq2. Genome Biol. *15*, 550.

Mani, S.A., Guo, W., Liao, M.J., Eaton, E.N., Ayyanan, A., Zhou, A.Y., Brooks, M., Reinhard, F., Zhang, C.C., Shipitsin, M., et al. (2008). The epithelial-mesenchymal transition generates cells with properties of stem cells. Cell *133*, 704–715.

Melino, G., Memmi, E.M., Pelicci, P.G., and Bernassola, F. (2015). Maintaining epithelial stemness with p63. Sci. Signal. *8*, re9.

Mills, A.A., Zheng, B., Wang, X.J., Vogel, H., Roop, D.R., and Bradley, A. (1999). p63 is a p53 homologue required for limb and epidermal morphogenesis. Nature *398*, 708–713.

Morris, R.J., Liu, Y., Marles, L., Yang, Z., Trempus, C., Li, S., Lin, J.S., Sawicki, J.A., and Cotsarelis, G. (2004). Capturing and profiling adult hair follicle stem cells. Nat. Biotechnol. *22*, 411–417.

Moustakas, A., and Heldin, P. (2014). TGFβ and matrix-regulated epithelial to mesenchymal transition. Biochim. Biophys. Acta *1840*, 2621–2634.

Nguyen, H., Rendl, M., and Fuchs, E. (2006). Tcf3 governs stem cell features and represses cell fate determination in skin. Cell *127*, 171–183.

Nguyen, H., Merrill, B.J., Polak, L., Nikolova, M., Rendl, M., Shaver, T.M., Pasolli, H.A., and Fuchs, E. (2009). Tcf3 and Tcf4 are essential for long-term homeostasis of skin epithelia. Nat. Genet. *41*, 1068–1075.

Nieto, M.A., Huang, R.Y., Jackson, R.A., and Thiery, J.P. (2016). EMT: 2016. Cell *166*, 21–45.

Ocaña, O.H., Córcoles, R., Fabra, A., Moreno-Bueno, G., Acloque, H., Vega, S., Barrallo-Gimeno, A., Cano, A., and Nieto, M.A. (2012). Metastatic colonization requires the repression of the epithelial-mesenchymal transition inducer Prrx1. Cancer Cell *22*, 709–724.

Paniz-Mondolfi, A., Singh, R., Jour, G., Mahmoodi, M., Diwan, A.H., Barkoh, B.A., Cason, R., Huttenbach, Y., Benaim, G., Galbincea, J., and Luthra, R. (2015). Cutaneous carcinosarcoma and the EMT: To transition, or not to transition? That is the question. Virchows Arch. *466*, 359–360.

Puisieux, A., Brabletz, T., and Caramel, J. (2014). Oncogenic roles of EMT-inducing transcription factors. Nat. Cell Biol. *16*, 488–494.

Rhim, A.D., Mirek, E.T., Aiello, N.M., Maitra, A., Bailey, J.M., McAllister, F., Reichert, M., Beatty, G.L., Rustgi, A.K., Vonderheide, R.H., et al. (2012). EMT and dissemination precede pancreatic tumor formation. Cell *148*, 349–361.

Robinson, J.T., Thorvaldsdóttir, H., Winckler, W., Guttman, M., Lander, E.S., Getz, G., and Mesirov, J.P. (2011). Integrative genomics viewer. Nat. Biotechnol. *29*, 24–26.

Siegel, P.M., and Massagué, J. (2003). Cytostatic and apoptotic actions of TGF-beta in homeostasis and cancer. Nat. Rev. Cancer *3*, 807–821.

Srinivas, S., Watanabe, T., Lin, C.S., William, C.M., Tanabe, Y., Jessell, T.M., and Costantini, F. (2001). Cre reporter strains produced by targeted insertion of EYFP and ECFP into the ROSA26 locus. BMC Dev. Biol. *1*, 4.

Tumbar, T., Guasch, G., Greco, V., Blanpain, C., Lowry, W.E., Rendl, M., and Fuchs, E. (2004). Defining the epithelial stem cell niche in skin. Science *303*, 359–363.

Tuveson, D.A., Shaw, A.T., Willis, N.A., Silver, D.P., Jackson, E.L., Chang, S., Mercer, K.L., Grochow, R., Hock, H., Crowley, D., et al. (2004). Endogenous oncogenic K-ras(G12D) stimulates proliferation and widespread neoplastic and developmental defects. Cancer Cell *5*, 375–387.

Vasioukhin, V., Degenstein, L., Wise, B., and Fuchs, E. (1999). The magical touch: Genome targeting in epidermal stem cells induced by tamoxifen application to mouse skin. Proc. Natl. Acad. Sci. USA *96*, 8551–8556.

Warzecha, C.C., Jiang, P., Amirikian, K., Dittmar, K.A., Lu, H., Shen, S., Guo, W., Xing, Y., and Carstens, R.P. (2010). An ESRP-regulated splicing programme is abrogated during the epithelial-mesenchymal transition. EMBO J. *29*, 3286–3300.

Watanabe, K., Villarreal-Ponce, A., Sun, P., Salmans, M.L., Fallahi, M., Andersen, B., and Dai, X. (2014). Mammary morphogenesis and regeneration require the inhibition of EMT at terminal end buds by Ovol2 transcriptional repressor. Dev. Cell *29*, 59–74.

Wellner, U., Schubert, J., Burk, U.C., Schmalhofer, O., Zhu, F., Sonntag, A., Waldvogel, B., Vannier, C., Darling, D., zur Hausen, A., et al. (2009). The EMT-activator ZEB1 promotes tumorigenicity by repressing stemness-inhibiting microRNAs. Nat. Cell Biol. *11*, 1487–1495.

White, A.C., Tran, K., Khuu, J., Dang, C., Cui, Y., Binder, S.W., and Lowry, W.E. (2011). Defining the origins of Ras/p53-mediated squamous cell carcinoma. Proc. Natl. Acad. Sci. USA *108*, 7425–7430.

Xiang, X., Deng, Z., Zhuang, X., Ju, S., Mu, J., Jiang, H., Zhang, L., Yan, J., Miller, D., and Zhang, H.G. (2012). Grhl2 determines the epithelial phenotype of breast cancers and promotes tumor progression. PLoS ONE *7*, e50781.

Yang, A., Schweitzer, R., Sun, D., Kaghad, M., Walker, N., Bronson, R.T., Tabin, C., Sharpe, A., Caput, D., Crum, C., and McKeon, F. (1999). p63 is essential for regenerative proliferation in limb, craniofacial and epithelial development. Nature *398*, 714–718.

Yang, J., Mani, S.A., Donaher, J.L., Ramaswamy, S., Itzykson, R.A., Come, C., Savagner, P., Gitelman, I., Richardson, A., and Weinberg, R.A. (2004). Twist, a master regulator of morphogenesis, plays an essential role in tumor metastasis. Cell *117*, 927–939.

Yang, H., Schramek, D., Adam, R.C., Keyes, B.E., Wang, P., Zheng, D., and Fuchs, E. (2015). ETS family transcriptional regulators drive chromatin dynamics and malignancy in squamous cell carcinomas. eLife *4*, e10870.

Zanconato, F., Forcato, M., Battilana, G., Azzolin, L., Quaranta, E., Bodega, B., Rosato, A., Bicciato, S., Cordenonsi, M., and Piccolo, S. (2015). Genome-wide association between YAP/TAZ/TEAD and AP-1 at enhancers drives oncogenic growth. Nat. Cell Biol. *17*, 1218–1227.

Zhang, B., Zhang, Z., Xia, S., Xing, C., Ci, X., Li, X., Zhao, R., Tian, S., Ma, G., Zhu, Z., et al. (2013). KLF5 activates microRNA 200 transcription to maintain epithelial characteristics and prevent induced epithelial-mesenchymal transition in epithelial cells. Mol. Cell. Biol. *33*, 4919–4935.

Zhang, X., Choi, P.S., Francis, J.M., Imielinski, M., Watanabe, H., Cherniack, A.D., and Meyerson, M. (2016). Identification of focally amplified lineage-specific super-enhancers in human epithelial cancers. Nat. Genet. *48*, 176–182.

Zhao, W., Wang, H., Han, X., Ma, J., Zhou, Y., Chen, Z., Zhou, H., Xu, H., Sun, Z., Kong, B., et al. (2016). DeltaNp63alpha attenuates tumor aggressiveness by suppressing miR-205/ZEB1-mediated epithelial-mesenchymal transition in cervical squamous cell carcinoma. Tumour Biol. *37*, 10621–10632.

Zhu, F., Park, E., Liu, B., Xia, X., Fischer, S.M., and Hu, Y. (2009). Critical role of IkappaB kinase alpha in embryonic skin development and skin carcinogenesis. Histol. Histopathol. *24*, 265–271.

STAR★METHODS

KEY RESOURCES TABLE

REAGENT or RESOURCE	SOURCE	IDENTIFIER
Antibodies		
Rabbit Polyclonal anti-Keratin 14	Thermo Fisher Scientific	N/A
Chicken anti-GFP	Abcam	ab13970
Rabbit anti-Sox 2 (clone EPR3131)	Abcam	ab92494, RRID: AB_10585428
Rabbit anti-Vimentin (clone EPR3776)	Abcam	ab92547, RRID: AB_10562134
Rat anti-ECadherin (clone DECMA-1)	eBioscience	# 503249
Polyclonal rabbit anti-p63	Santa Cruz	N/A
Polyclonal Rabbit anti-Zeb1	Bethyl	IHC-00419, RRID: AB_1659852
Polyclonal Rabbit anti-Zeb2	Sigma Aldrich	HPA003456, RRID: AB_10603840
Polyclonal Rabbit anti Epcam	Abcam	ab71916
Anti chicken Alexa Fluor 488	Molecular Probes	A-11039, RRID: AB_142924
Anti Rabbit rhodamine Red-X	Jackson ImmunoResearch	# 111-295-003, RRID:AB_2338022
Anti Rat Cy5	Jackson ImmunoResearch	# 112-175-167, RRID:AB_2338264
Rat PE-conjugated anti-CD45 (clone 30F11)	eBioscience	# 12-0451
Rat PE-conjugated anti CD31 (clone MEC13.3)	BD	# 553373
APC-Cy7-conjugated anti-Epcam (clone G8.8)	Biolegend	# 624073
Chemicals, Peptides, and Recombinant Proteins		
Collagenase I	Sigma	C0130
Mouse recombinant TGF-β1	R&D Systems	Cat #76 66-MB
Mouse recombinant TGF-β2	R&D Systems	Cat #7346-B2
Puromycin	InvivoGen	Ant-pr-1
Polybrene	Millipore	TR-1003-G
Critical Commercial Assays		
Nextera DNA Library preparation kit	Illumina	FC-121-1030
Nextera Index Kit	Illumina	FC-121-1011
MinElute purification kit	QIAGEN	Cat # 28004
Vectastain Elite ABC HRP Kit (Peroxidase, Standard)	Vector Laboratories	Cat # PK-6100
ImmPACT DAB	Vector Laboratories	Cat # SK-4105
Ovation® SoLo RNA-Seq System	NuGEN	Part # 0501-32
RNeasy micro kit	QIAGEN	Cat # 74004
Deposited Data		
Mouse reference genome GRCm38.p4/mm10	Genome Reference Consortium	http://www.ncbi.nlm.nih.gov/grc/mouse
Microarrays, ATAC-seq, and RNA-seq data	This paper	GEO: GSE88989
Experimental Models: Cell Lines		
HEK293T	ATCC	CRL-3216
3T3	ATCC	CRL-6361
Experimental Models: Organisms/Strains		
Rosa26-YFP	Jackson Labs	# 006148
K14CreER	Jackson Labs	# 005107
Lgr5CreER	Jackson Labs	# 008875
KRas$^{LSL-G12D}$	Jackson Labs	NCI 01XJ6
p53$^{fl/fl}$	Jackson Labs	# 008462
NOD/SCID/Il2Rγ null	Charles River	N/A

(Continued on next page)

REAGENT or RESOURCE	SOURCE	IDENTIFIER
Rosa26-ΔNp63-IRES-GFP	Wim Declercq lab	N/A
Recombinant DNA		
Packaging plasmid psPax2	Addgene	Cat #12260
VSV-G envelope expressing plasmid pMD2.G	Addgene	Cat #12259
Sequence-Based Reagents		
Primers for recombinaison PCR **Cre**: Fwd 5′-3′: TGCTGTTTCACTGGTTATGCGG	This paper	N/A
Cre: Rv 5′-3′: TTGCCCCTGTTTCACTATCCAG	This paper	N/A
KrasG12D: Fwd 5′-3′: GTCTTTCCCCAGCACAGTGC	This paper	N/A
KrasG12D: Rv 5′-3′:CTCTTGCCTACGCCACCAGCTC	This paper	N/A
p53flox: Fwd 5′-3′: CAGAAAAACAGGTTAAACCCAG	This paper	N/A
p53flox: Rv 5′- 3′: AGCACATAGGAGGCAGAGAC	This paper	N/A
Primers for qPCR, see Table S2	This paper	N/A
shRNA targeting sequence, see Table S2	Sigma Aldrich	N/A
Software and Algorithms		
Axiovision	Carl Zeiss Inc	N/A
FACSDiva software	BD Bioscience	N/A
Extreme limiting dilution analysis (ELDA) software	Hu and Smyth, 2009	http://bioinf.wehi.edu.au/software/elda/
Light Cycler ® 96	Roche	N/A
Bowtie2 version 2.2.3	Langmead and Salzberg, 2012	http://bowtie-bio.sourceforge.net/bowtie2/index.shtml
R Bioconductor gplots		http://CRAN.R-project.org/package=gplots
R Bioconductor package DESeq2	Love et al., 2014	http://www.bioconductor.org/packages/release/bioc/html/DESeq2.html
HOMER package findMotifsGenome.pl	Heinz et al., 2010	http://homer.salk.edu/homer/ngs/peakMotifs.html

CONTACT FOR REAGENT AND RESOURCE SHARING

Further information and requests for reagents may be directed to, and will be fulfilled by, the Lead Contact, Pr. Cédric Blanpain (Cedric.blanpain@ulb.ac.be).

EXPERIMENTAL MODEL AND SUBJECT DETAILS

Mice

Rosa26-YFP (Srinivas et al., 2001), K14CreER (Vasioukhin et al., 1999), Lgr5CreER (Barker et al., 2007), KRas$^{LSL-G12D}$ (Tuveson et al., 2004) and p53$^{fl/fl}$ (Jonkers et al., 2001) mice have been imported from the NCI mouse repository and the Jackson Laboratories. Wim Declercq (Ghent University, Belgium) generated the Rosa26-ΔNp63-IRES-GFP. NOD/SCID/Il2Rγ null mice were purchased from Charles River.

All mice used in this study were composed of males and females with mixed genetic background. Mouse colonies were maintained in a certified animal facility in accordance with the European guidelines and with approved ethical protocol (#483N).

Primary cell culture

FACS isolated tumor YFP+EpCam+ or Epcam- cells were plated on γ-irradiated 3T3 feeder cells in 6-well plates. Cells were cultured in MEM medium supplemented with 10% FBS, 0.4 μg/ml hydrocortisone, 10 ng/ml EGF, 2x10^{-9}M T3, 1% penicillin/streptomycin, 2mM L-glutamine. The feeders were removed using PBS/EDTA (1mM). Cells are incubated at 37°C with 20% O$_2$, and 5% CO$_2$.

METHOD DETAILS

No randomization or blinding was performed in this study. Sample-size and statistical methods are indicated in the quantification and statistical analysis paragraph.

KRasG12D p53fl/fl induced skin tumors

Tamoxifen (TAM) was diluted at 25 mg/ml in sunflower oil (Sigma). 2,5 mg TAM was administered intraperitoneally (IP) to K14CreER/KRas$^{LSL-G12D}$/p53$^{fl/fl}$/Rosa-YFP$^{+/+}$ mice while Lgr5CreER/KRas$^{LSL-G12D}$/p53$^{fl/fl}$/Rosa-YFP$^{+/+}$ and Lgr5CreER/KRas$^{LSL-G12D}$/p53$^{fl/fl}$/Rosa26-ΔNp63-IRES-GFP mice were treated with 4 daily IP doses of 2,5 mg of TAM at P28 as previously described (Lapouge et al., 2012; Lapouge et al., 2011). 1 mg of TAM was given to reduce the number of tumors in Lgr5CreER model.

Monitoring of tumor growth

Tumor appearance and size were detected by daily observation and palpation. Mice were euthanized when tumor size reached 1cm^3 or when mice presented signs of distress. Skin tumors were measured using a precision calliper allowing to discriminate size modifications > 0,1mm. Tumor volumes were measured the first day of appearance of the tumor and then, every week until the death of the animal with the formula V = π x [d^2 x D] / 6, where d is the minor tumor axis and D is the major tumor axis.

Antibodies

The following primary antibodies were used: anti-K14 (polyclonal rabbit, 1:1000, Thermo Fisher Scientific), anti-GFP (chicken, 1:1000, Abcam), anti-SOX2 (rabbit, 1:100, Abcam), anti-Vimentin (Rabbit, 1:200, Abcam), Anti-ECadherin (rat, clone DECMA-1, 1:1000, eBioscience), anti-p63 (polyclonal rabbit, 1:200, Santa Cruz), Anti-Zeb1 (polyclonal rabbit, 1:300, Bethyl), Anti-Zeb2 (polyclonal rabbit, 1:200, Sigma), anti-EpCam (rabbit polyclonal, 1:200, Abcam). The following secondary antibodies were used: anti-rabbit, anti-rat, anti-chicken, conjugated to AlexaFluor488 (1:400, Molecular Probes), to rhodamine Red-X or to Cy5 (1:400, Jackson ImmunoResearch).

Histology and immunostaining

For the staining on frozen sections, tissues were pre-fixed in 4% paraformaldehyde during 2 hr at room temperature, then washed in PBS, incubated overnight in 30% sucrose at 4°C, and embedded in OCT (Tissue Tek) for cryopreservation. Samples were sectioned at 5 μm sections using CM3050S cryostat (Leica Microsystems GmbH). Nonspecific antibody binding was blocked with 5% horse serum, 1% BSA, and 0.2% Triton X-100 during 1 hr. Primary antibodies were incubated overnight at 4°C in blocking buffer. Sections were rinsed in PBS and incubated with secondary antibodies during 1 hr at room temperature. Nuclei were stained with Hoechst (4 mM). Slides were mounted using Glycergel (Dako) supplemented with 2.5% DABCO (Sigma-Aldrich).

For the staining on paraffin sections (for Sox2, Zeb1, Zeb2 and YFP antibodies), 4 μm paraffin sections were deparaffinized and rehydrated. Antigen unmasking was performed in citrate buffer (pH 6) at 98°C during 20 min using the PT module. Endogenous peroxydase was blocked using 3% H$_2$O$_2$ (Merck) in methanol (VWR) during 20 min at room temperature. Endogenous avidin and biotin were blocked using the Endogenous Blocking kit (Invitrogen) during 20 min at room temperature. Primary antibodies were incubated overnight at 4°C. Anti-rabbit biotinylated secondary antibodies were used, as well as Standard ABC kit, and ImmPACT DAB (Vector Laboratories) for the detection of HRP activity. Slides were mounted using SafeMount (Labonord).

Image acquisition

Imaging was performed on a Zeiss Axio Imager M1 (Thornwood) fluorescence microscope with a Zeiss Axiocam MR3 camera and a Zeiss Axiocam MRC5 camera for bright-field microscopy using Axiovision release 4.6 software. Brightness, contrast, and picture size were adjusted using Photoshop CS6 (Adobe).

FACS Isolation of TECs and TMCs

Tumors were dissected, minced and digested in collagenase I (Sigma) during 2 hr at 37°C on a rocking plate. Collagenase I activity was blocked by the addition of EDTA (5 mM) and then the cells were rinsed in PBS supplemented with 2% FBS. Before the staining, cells were blocked during 20 min at room temperature in PBS supplemented with 30% FBS. Cell suspensions were filtered through a 70 μm cell strainers (BD) then through a 40 μm cell strainer to ensure the elimination of cell debris and clumps of cells. Immunostaining was performed using PE-conjugated anti-CD45 (clone 30F11, 1:100, eBioscience), PE-conjugated anti CD31 (clone MEC13.3; 1:100, BD PharMingen), and APC-Cy7-conjugated anti-Epcam (clone G8.8; 1:100, Biolegend), during 30 min at 4°C on a rocking plate. Living tumor cells were selected by forward scatter, side scatter, doublets discrimination and by Hoechst dye exclusion. EpCam+ and EpCam- tumor cells were selected based on the expression of YFP and the exclusion of CD45, CD31 (Lin-). Fluorescence-activated cell sorting analysis was performed using FACSAria and FACSDiva software (BD Bioscience). Sorted cells were collected either in culture medium for in vivo transplantation experiments or into lysis buffer for RNA extraction.

Tumor transplantation assays

The different FACS isolated populations of tumor cells (YFP+ Epcam+ from K14CreER and YFP+ EpCam+ from Lgr5CreER) were collected in 4°C medium. Cells at different dilutions (1000 / 100 / 10 cells) were resuspended in 50 μl of Matrigel (50 μl, E1270, 970 mg/ml; Sigma) and injected subcutaneously to NOD/SCID/Il2Rγ null mice (Charles River, France). Triplicate injections per mouse were performed. Secondary tumors were detected by palpation every week and their size monitored until tumor reached 1cm^3 or when mice presented signs of distress, and the mice were sacrificed.

In vitro TGF-β treatment

FACS isolated tumor YFP+EpCam+ cells were plated on γ-irradiated 3T3 feeder cells in 6-well plates. For stimulation experiments, media were supplemented with recombinant mouse TGF-β1 and TGF-β2 (10ng/ml) (catalog number #76 66-MB and #7346-B2 respectively, R&D Systems; resuspended with 4mM HCl, 0,1% BSA).

Virus production, infection and selection

Stable knockdown cell lines were generated using lentiviral pLKO/PuroR vectors (Sigma) after puromycin selection (2,5 μg/mL for TECs and 10 μg/mL for TMCs). Knockdown was confirmed by qRT-PCR. Three different shRNA were used at the same time to target the same gene. The list of all the shRNA used is listed in Table S2.

For virus production, 5x10⁶ HEK293T cells were seeded into 10 cm dishes and transfected with the vector of interest and appropriate packaging plasmids psPax2 and pMD2.G (#12260 and #12259 respectively, Addgene). Medium was changed 24 hr later and next, supernatants were collected at 48 hr, and passed through a 0.45 μm filter. TECs of TMCs were plated in 6-well plate cells and incubated with 40 μl/ml viruses when they reach 50% of confluence, in the presence of polybrene (5 μg/ml). Medium was changed 24 hr later and cells were selected with Puromycin for at least1 week.

RNA and DNA extraction, real-time PCR

RNA extraction from FACS isolated cells was performed using the RNeasy micro kit (QIAGEN) according to the manufacturer's recommendations with DNAase treatment. After nanodrop RNA quantification, the first strand cDNA was synthesized, using Superscript II (Invitrogen) and random hexamers (Roche) in 50μl final volume. Control of genomic contaminations was measured for each sample by performing the same procedure with or without reverse transcriptase. Quantitative PCR assays were performed using 1 ng of cDNA as template, SYBRGreen mix (Applied Bioscience) and an Light Cycler ® 96 (Roche) real-time PCR system. TBP housekeeping gene was used for normalization. Primers were designed using Roche Universal ProbeLibrary Assay Design Center (https://lifescience. roche.com/webapp/wcs/stores/servlet/CategoryDisplay?tab=Assay+Design+Center&identifier=Universal+Probe+Library&langId=-1) and are presented in Table S2. Quantitative PCR Analysis was performed using Light Cycler ® 96 (Roche) and the DDCt method with TBP as a reference.

Microarray analysis

Total RNA was analyzed using Mouse whole genome 430 2.0 array from Affymetrix at the AROS Applied Biotechnology A/S microarray facility (Aros, Denmark) and Mouse whole genome 430 PM at IRB Functional Genomics Core (Barcelona, Spain). 4 different biological replicates of FACS isolated YFP+ EpCam+ cells from K14 tumors, 4 biological replicates of FACS isolated YFP+ EpCam+ cells from Lrg5 mixed SCCs, 4 biological replicates of FACS isolated YFP+ EpCam− cells, from Lgr5 mixed SCCs, 2 biological replicates of FACS isolated YFP+ EpCam+ cells from Lgr5 ΔNp63 and 2 biological replicates of FACS isolated YFP+ EpCam- cells from Lgr5 ΔNp63 were analyzed. Cells from Interfollicular Epidermis and infundibulum (Lgr5-GFP negative, α6HCD34-) and Lgr5-GFP+ Hair Follicle cells have been FACS sorted before KRasG12D p53cKO recombinaison and 2 biological replicates of each case were analyzed.

All the results were normalized using the fRMA normalization using R-bioconductor package fRMA with standard parameters. Cross platform normalization was further performed to eliminate the batch effect using ComBat unsupervised clustering using the Surrogate Variable Analysis, and heatmap was generated using gplots (http://CRAN.R-project.org/package=gplots), all in R-bioconductor.

ATAC-seq

Assay for transposase accessible chromatin (ATAC) followed by sequencing was performed as following: 100000 sorted cells were collected in 1mL of PBS+3%FBS at 4°C. Cells were centrifuged, then cell pellets were resuspended in 50 μL of lysis buffer (Tris HCl 10mM, NaCl 10mM, MgCl2 3mM, Igepal 0,1%) and centrifuged (500 g) for 25 min at 4°C. Supernatant was discarded and nuclei were resuspended in 50 μL of reaction buffer (Tn5 transposase 2,5 μL, TD buffer 22,5 μL and 25 μL H2O – Nextera DNA sample preparation kit, Illumina). The reaction was performed for 30 min at 37°C and then blocked by addition of 5uL of clean up buffer (NaCl 900mM, EDTA 300mM). DNA was purified using the MinElute purification kit (QIAGEN).

Library preparation and sequencing

DNA libraries were PCR amplified (Nextera DNA Sample Preparation Kit, Illumina), and size selected for 200 to 800 bp (BluePippin, Sage Sciences), following manufacturers' protocols.

Alignment and Peak calling

More than 50 000 000 reads were mapped to mouse genomic DNA in each condition. ATAC-seq reads (single-end or paired-end) were aligned to mouse genome (NCBI37/mm10) using Bowtie2 (version 2.2.3) (Langmead and Salzberg, 2012) using option of "–local" for single-end and "–local–very-sensitive-local–dovetail–dovetail -X 1000" for paired-end. Mitochondrial reads were excluded from downstream analysis and duplicate reads were removed by Picard tools (http://broadinstitute.github.io/picard/). Alignment data tracks were visualized by Integrative Genomics Viewer (IGV) (Robinson et al., 2011).

Peak calling was performed on each individual sample by HOMER (Heinz et al., 2010) with parameters setting of "-L 0 -C 3 -size 1000 -minDist 1000 -tbp 3 -o auto." Peaks from different ATAC-seq samples were merged for downstream analysis.

Differential Peak analysis

Pairwise comparisons of ATAC peaks between two conditions were performed by R package DESeq2 (Love et al., 2014), with reads count of each peak calculated by HTSeq-count (Anders et al., 2015). Significance is defined as adjusted p value smaller than 0.001 and fold change more than 3. Peaks were assigned to the nearest Refseq annotated genes with 500kb range.

Motif analysis

De novo motif search was performed using program of findMotifsGenome.pl in the HOMER package (Heinz et al., 2010) with parameters setting of "-size −250,250 -S 15 -len 6,8,10,12,16." Incidences of specific motif was examined by the program of annotatePeaks.pl in the HOMER package with size parameter "-size 500."

GSEA analysis

GSEA analysis was performed using ranked fold change values (Epcam- over Epcam+) of ATAC peaks for the displayed dataset. For the upregulated or downregulated genes, the highest fold change peak was selected to represent the gene and enrichment score was calculated following GSEA documentation.

RNA sequencing

RNA quality was checked by Bioanalyzer (Agilent). For RNA extracted from TECs or TMCs, indexed cDNA libraries were obtained using the Ovation Solo RNA-Seq Systems (NuGen) following manufacturer recommendations. The multiplexed libraries (11 pM) were loaded and sequences were produced using a HiSeq PE Cluster Kit v4 and TruSeq SBS Kit v3-HS (250 cycles) on a HiSeq 1500 (Illumina). Approximately 8 million of paired-end reads per sample were mapped against the mouse reference genome (GRCm38.p4/mm10) using STAR software to generate read alignments for each sample. Annotations Mus_musculus.GRCm38.84.gtf were obtained from ftp. Ensembl.org. After transcripts assembling, gene level counts were obtained using HTSeq and normalized to 20 millions of aligned reads. Fold of changes (FC) were computed on these values between the conditions.

QUANTIFICATION AND STATISTICAL ANALYSIS

Estimation of tumor propagating cell frequency

The frequency of tumor propagating cells was calculated using the extreme limiting dilution analysis (ELDA) online software as previously described (http://bioinf.wehi.edu.au/software/elda/) (Hu and Smyth, 2009). The statistical p value was obtained using a Chi-square test.

Statistics

Statistical and graphical data analyses were performed using Prism 5 (Graphpad) software. All experiments shown were replicated at least twice. All data in histograms represent mean ± SEM. Data of tumor propagating cells frequencies (Figure 2B) represent percentage with 95% confidence interval. Data were tested for normality using either D'Agostino and Pearson omnibus normality test or Kolmogorov-Smrinov test (with Dallal-Wilkinson-Lilliefor P value). Statistical significance was calculated by Mann-Whitney test when sample size was small (Figures 1C, 1H, 2G, 5H, 7D, S1C, S1D, and S1G), by Wilcoxon matched paired signed rank test for non-parametric paired data (Figures S1J and S4Q–S4T), by Fisher's exact test for analysis of proportions (Figure 1I) and by Log-Rank test for ranked observations (Figure S1E). Chi square test for analysis of proportions when n is large (Figure 2B) using the Graphpad Prism 6 software, considering p < 0.05 as statistically significant. All tests are two-sided.

DATA AND SOFTWARE AVAILABILITY

The accession number for the microarray data, RNA sequencing, and ATAC sequencing reported in this paper is GEO: GSE88989.

ADDITIONAL RESOURCES

Annotations of Mus_musculus.GRCm38.84.gtf were obtained from ftp.Ensembl.org.